Journal of Structural Geology 32 (2010) 1609–1628

Contents lists available at ScienceDirect

Journal of Structural Geology

journal homepage: www.elsevier.com/locate/jsg

Extensional faults in fine grained carbonates – analysis of fault core lithology and thickness–displacement relationships

Eivind Bastesen [a,b,*], Alvar Braathen [b,c]

[a] Centre for Integrated Petroleum Research, University of Bergen, 5020 Bergen, Norway
[b] Department of Earth Science, University of Bergen, 5020 Bergen, Norway
[c] University Centre in Svalbard, 9171 Longyearbyen, Norway

ARTICLE INFO

Article history:
Received 4 July 2009
Received in revised form
26 August 2010
Accepted 18 September 2010
Available online 25 September 2010

Keywords:
Thickness–displacement
Extensional faults
Carbonates
Fault core
Fault facies

ABSTRACT

A study of 103 extensional faults hosted by fine grained carbonates in western Sinai, Svalbard and Oman reveals that faults vary geometrically between simple cores and cores comprising fault splays, lenses, segment linkages and overlap structures. Fault core rocks are typically carbonate breccias, carbonate and shale gouge, shale smear, secondary calcite cement and veins, and host rock lenses.

There is a significant scatter in the core thickness for any given displacement, but the overall pattern is that the thickness increases with displacement. This increase best fits a power law function ($0.29D^{0.56}$) that describes a gradual decrease in the thickness/displacement relationship for increasing slip along faults. In more detail, the general function can be seen as the sum of two (power law) trend lines; the first representing thin localized fault cores with generally simple and planar geometry, the second representing thicker fault cores with complex geometry of lenses and overlap structures and with fault rock membranes.

The studied faults show a significant change in composition and geometry from small (0–1 m), to moderate (1–10 m) and to large offset faults (10–400 m). The overall pattern is that fault initiates as fractures filled with calcite veins and thin shear fractures that hosts gouge membranes. With increased fault offset, complexity increases with breakdown of veins, more extensive fault rock membranes, and a trend towards development of lenses. When offset exceeds 100 m, cores become complex, with multiple slip zones, cemented breccia and shale smear membranes, and various types of lenses. We envision that the fault development as reflected by offset is dominated by forces (extension, compression) acting in the fault, mechanical heterogeneity of wall rocks, the core lithologies and their developing rheology, and especially geometric effects arising from fault irregularities.

1. Introduction

Characterization and quantification of fault zones in outcrops is a fundamental requirement for modelling and forecasting structural reservoir heterogeneity in carbonate reservoirs. Key parameters for fault characterization include fault thickness, composition, geometry and displacement (e.g. Yielding et al., 1997; Manzocchi et al., 1999; Braathen et al., 2009). A fault can be defined as a zone of focused deformation that can be subdivided into domains/subzones termed "core" and "damage zone(s)" (e.g. Chester and Logan, 1986). Alternatively, a fault can be considered an array of hard-linked and soft-linked fault segments of various scales that affect a restricted rock volume or "fault envelope" (e.g. Peacock, 2002; Childs et al., 2009; Braathen et al., 2009). Descriptions of fault cores (e.g. Caine et al., 1996; Childs et al., 1996; Lindanger et al., 2007; Bonson et al., 2007; Wibberley et al., 2008; Bastesen et al., 2009; Braathen et al., 2009) show a number of recurring elements such as slip surfaces, fracture/deformation band sets, fault rocks (gouge, breccias and cataclasites), shale smears, and lenses of protolith or fault rock. Bulk strain of the core is semi-penetrative to penetrative, and core elements in most cases exhibit significantly altered fluid conductivity compared to the host rock from which they are derived. In contrast, bulk strain in the damage zones flanking the core is non-penetrative and hosts discrete structures including minor faults, fractures and/or deformation band sets. Studies addressing the width of the fault zone envelope vs. fault displacement have revealed a substantial degree of variation and uncertainty (e.g. Hull, 1988; Knott, 1994; Shipton et al., 2006; Childs et al., 2009). In most cases the thickness/displacement ratio (T/D) shows that thickness

* Corresponding author. Centre for Integrated Petroleum Research, Uni Research, 5020 Bergen, Norway. Tel.: +47 99230248.
E-mail address: Eivind.bastesen@Uni.no (E. Bastesen).

0191-8141/$ – see front matter © 2010 Elsevier Ltd. All rights reserved.
doi:10.1016/j.jsg.2010.09.008

varies by up to three orders of magnitude for a given displacement, reflecting the geometric complexity arising from the presence of linked and unlinked segments (Childs et al., 2009).

In this paper we present characteristics and scaling laws for faults in fine grained carbonates. The dataset includes 103 faults described using the fault facies characterization concept (Braathen et al., 2009). Fault facies refers to any feature or rock body deriving its properties from tectonic deformation (Tveranger et al., 2005), and includes the main elements such as lenses, membranes and fractures. Fault facies can be characterized in terms of dimensions, geometry, internal structure and petrophysical properties, thus facilitating quantification, pattern recognition and statistical handling of structural elements in fault envelopes (Tveranger et al., 2005; Braathen et al., 2009). In the present study we have defined fault facies according to composition and geometry. Fault core geometry and distribution of fault facies are analysed in relation to the T/D ratio as established for each studied fault.

Fault architecture and related fluid flow properties in carbonate rocks have in the last years received increased attention (e.g. Agosta and Kirschner, 2003; Cello et al., 2003; Micarelli et al., 2003; Storti et al., 2003; Labaume et al., 2004; Agosta and Aydin, 2006; Graham Wall et al., 2006; Bonson et al., 2007; Benedicto et al., 2008; Bastesen et al., 2009; Putz-Perrier and Sanderson, 2010). However, studies addressing scaling relationships of faults in such rocks are scarce, and restricted to faults with small displacements (Billi et al., 2003; Micarelli et al., 2006; Soliva and Benedicto, 2005), or case studies (Micarelli et al., 2003; Agosta and Aydin, 2006; Bonson et al., 2007; Bastesen et al., 2009). In this paper we present a database of extensional faults from shallow buried (<2 km) carbonates from three different regions: western Sinai (Egypt), Central Spitsbergen, Svalbard (Arctic Norway), and Central Oman (Adams Foothills). The bulk of the data were collected in western Sinai, whereas data from Spitsbergen and Oman were collected for comparison purposes (i.e. different tectonic regimes and/or protoliths). All three areas exhibit thick successions of sedimentary carbonates which are truncated by well exposed extensional faults at different scales, with fault displacements ranging from a few centimetres to several hundred metres. In Sinai (e.g. Moustafa, 2004) and Spitsbergen (e.g. Steel and Worsley, 1984; Maher and Braathen, in press), faulting is related to regional rifting events, whereas in Oman, extensional faults are found along the crest of regional anticlines and domes, of which the folding is controlled by deep-seated thrusting and salt movements (e.g. Hanna, 1990). Protoliths range from massive homogenous limestone to layered heterogeneous shale-rich carbonates and marls.

2. Terminology

The studied fault cores exhibit several fault core facies associations (Braathen et al., 2009), which allow an identification and a description of fault facies using lithology and fault core geometry as descriptive parameters. Lithologically, fault core facies associations can be subdivided into shale smear (SS) (Lindsay et al., 1993; Yielding et al., 1997), carbonate breccia (CB) (Billi, 2005; Micarelli et al., 2003, 2006), secondary calcite (SCa) (Benedicto et al., 2008), or composite cores; the latter displaying two or all three fault core facies associations (Fig. 1).

The fault rocks observed in the present study formed at shallow depths and at low temperature, and in most cases bear resemblance to the primary non-cohesive breccia series described by Sibson (1977) and Braathen et al. (2004). Clast materials are fragments of carbonate formed by brittle failure. The breccia matrix consists of either finely crushed limestone fragments in a gouge (mud fraction fault rock), fine breccia (Billi, 2005) exhibiting varying degrees of cementation (CB), or shale; the latter giving rise to shale supported breccias (SCB) (Fig. 1b,c). In this study gouge was observed as very fine, crushed carbonate material and thin (<1 mm) membranes of sheared calcareous clay along faults. Shale smears are shale layers dragged into the fault, aligned parallel to fault dip and connected to a source shale layer (Lindsay et al., 1993). Secondary mineral precipitation was observed in the shape of calcite veins and void fillings and as pore space fill in breccias (described above). In many places precipitated calcite forms fault-parallel membranes and lenses, displaying the typical crack-seal vein appearance advocated by Petit et al. (1999). In the following descriptions the compositional elements are arranged into fault facies such as lenses (Childs et al., 1997; Gabrielsen and Clausen, 2001) and membranes (Braathen et al., 2009). Fault lenses are elongate pods of host rocks, fault rocks and/or calcite veins which are completely separated from the surrounding fault elements by slip surfaces with wall rocks (slip zones) (Fig. 1a). Membranes are continuous, semi-continuous or patchy fault-parallel sheets consisting of carbonate breccias, gouge, shale smear or veins.

Overall fault geometries are classified in Fig. 2. The Type 1 geometry corresponds to faults with a simple geometry, which further divides into planar geometry (1a) or fault cores that exhibit jogs or bends of either releasing (1b) or restraining (1c) character. Secondary shear fractures are classified according to their slip direction relative to the main fault orientation (Petit, 1987; Bastesen et al., 2009). These are termed R, P or R′ shears and correspond to Type 2 a, b and c, respectively. Type 3 geometries are soft-linked releasing (3a) or restraining (3b) overlap structures (Rykkelid and Fossen, 2002; Ferrill and Morris, 2003), while Type 4 geometries represent breached relays. Fault lenses are assigned to the Type 5. The Type 6 geometry includes faults with multiple slip surface zones, several lenses and complex intrinsic composition.

3. Methods

3.1. Database

The database analysed in this study includes a total of 103 extensional faults: 68 from western Sinai, 22 from Oman and 13 from Central Spitsbergen. Fault displacements range from 2.6 cm to 400 m, and fault core thicknesses from 1 mm to 11 m. For the purpose of the present study, faults are termed “small” when the displacement is smaller than 1 m, “moderate” when the displacement is in the range of 1–10 m, and “large” for the range of 10–400 m. The faults are mainly exposed in 2D cliff sections. For each fault core thickness, composition and the overall geometry were recorded (Figs. 1 and 2). The thickness was measured normal to the dip of the fault. Due to along-fault variations, the thickness was measured in several places along individual fault outcrops, covering the maximum and minimum thicknesses of the fault. This yielded a database of 423 thickness points for a given displacement, with assigned composition and geometry.

3.2. Fault core thickness

The precise boundaries of the fault core are in some cases difficult to establish accurately (Childs et al., 2009). In such cases we define the core as the part of the fault envelope accommodating the bulk of the displacement and delimits it by identifying intervals where sedimentary structures are significantly displaced (lenses) or pervasively deformed (brecciated). The core can also consist entirely of precipitated calcite along one or more fractures (Fig. 1a). In some cases, the fault core and host rock are separated by a slip surface, in other cases this transition may be gradual, forming

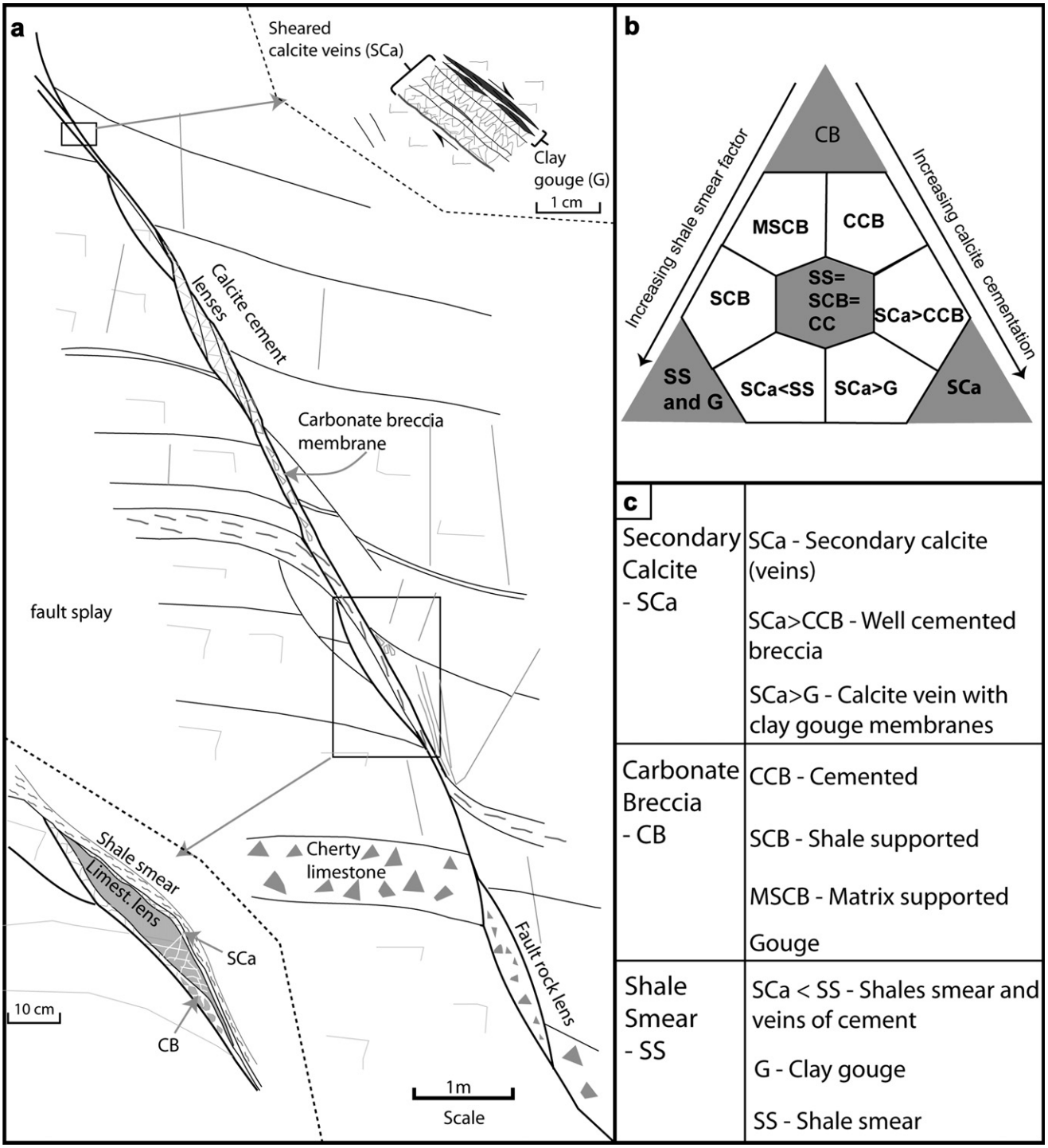

Fig. 1. a) Schematic fault core with lithologies and geometries typically encountered in small to moderate offset extensional faults in fine grained carbonates. The fault core area is defined by the bold lines, whereas the surrounding rock is deformed in the damage zone. The upper part of the fault core consists mainly of calcite veins and shale gouge (see inset), where the calcite veins are truncated by slip surfaces coated with gouge to form sheared calcite veins and lenses. The middle part of the core is dominated by membranes of carbonate breccias, while the lower part hosts shale smear and associated breccias that are arranged in composite lenses. b) Ternary compositional facies diagram based on three end members; shale smear (SS), secondary calcite (SCa) and carbonate breccia (CB). Fault cores with combinations of these elements are represented within the diagram. In cases where all three elements are observed, the fault core is described as a composite facies core that plots in the middle of the diagram. c) Table explaining the abbreviations of the fault core composition.

a fault core-damage zone transition (Billi et al., 2003). Relay structures and fault bends require additional criteria, in that they offer increased complexity. Breached relays were measured as single fault strand; in un-breached relays the two fault strands were measured individually.

3.3. Fault displacement

Measuring displacement is fairly straightforward, in cases where the fault displacement does not exceed the height of the outcrop. For larger faults, with displacements exceeding the height

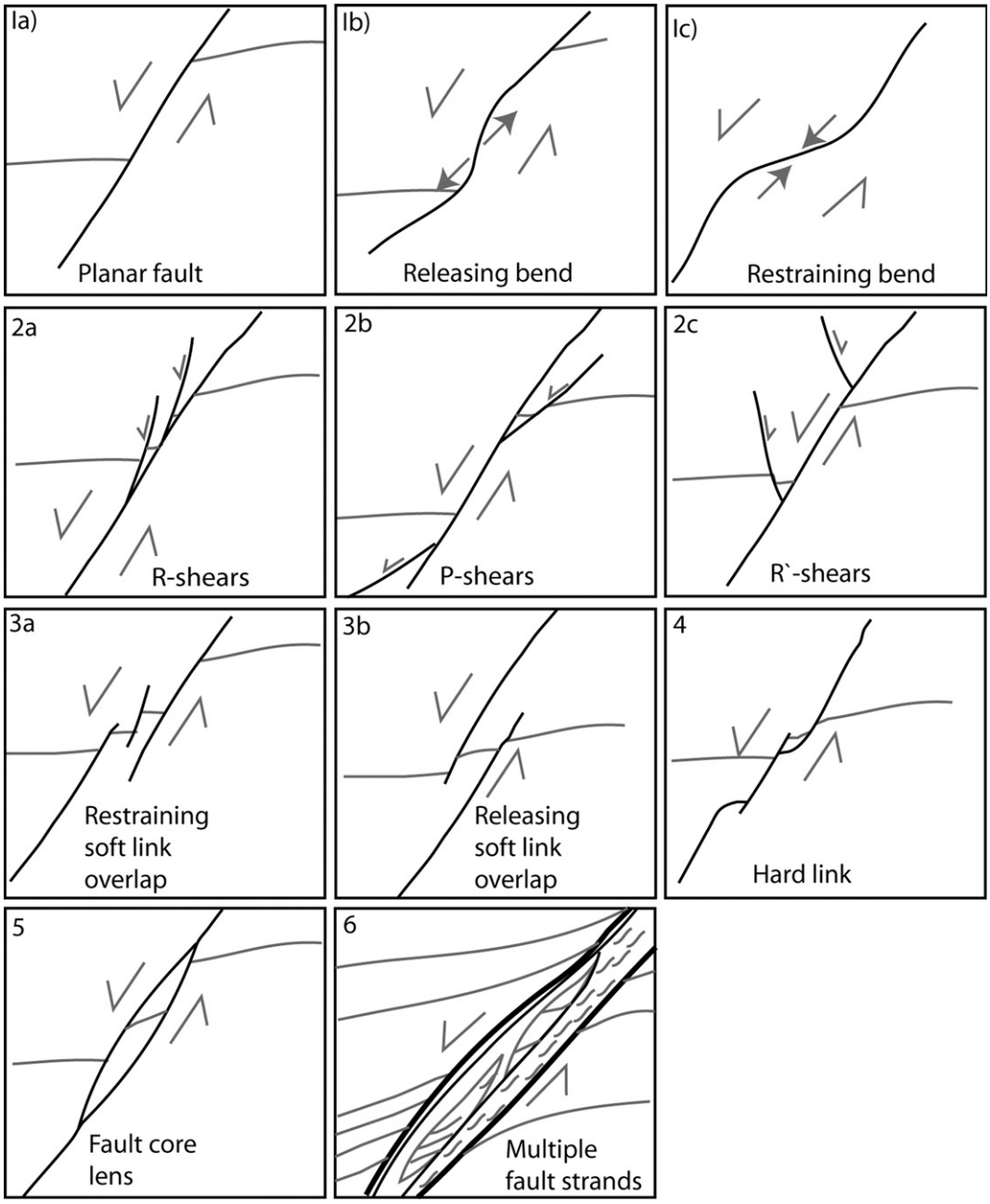

Fig. 2. Geometric classification scheme, showing possible geometries encountered in extensional faults. The diagram spans from planar faults (1a) to fault with complexities; such as fault bends (1b,c), complex faults with splay structures (2), overlap structures (3), breached overlap (4), lenses (5), and multiple fault strands (6).

of the exposure, local and/or regional stratigraphy and formation thickness data must be used. Thus stratigraphic offset can be estimated by applying the overall geometry of the fault, such as dip, position of relay structures, and fault drag. The accuracy of this method is dependent on the level of stratigraphic details available and, consequently, the precision of the estimated displacement commonly decreases with increasing displacement.

4. Geological setting

4.1. Western Sinai

The studied faults are located in carbonates exposed in the eastern, exhumed flank of the Suez Rift (Figs. 3a and 4). The region is characterized by large fault blocks (e.g. Hammam Faraoun and El Qaa) bounded by basement-involved, west-facing extensional master faults (Coastal fault belt and Eastern boundary fault belt) with kilometre-scale displacement (Moustafa and Abdeen, 1992; Sharp et al., 2000; Jackson et al., 2006). These large fault blocks are broken up by subsidiary faults with maximum displacement of a few hundred metres. The main period of fault movement, as recorded by syn-rift deposits, occurred during the Oligocene to mid-Miocene (e.g. Robson, 1971; Patton et al., 1994; Bosworth et al., 2005). Faults included in the present database were found in the Hammam Faraoun and El Qaa fault blocks (Fig. 4a).

Carbonates form a substantial part of the ~500 m thick late Cretaceous to early Tertiary El Egma Group (Moustafa and Abdeen, 1992; Bosworth et al., 2005), which can be further subdivided into

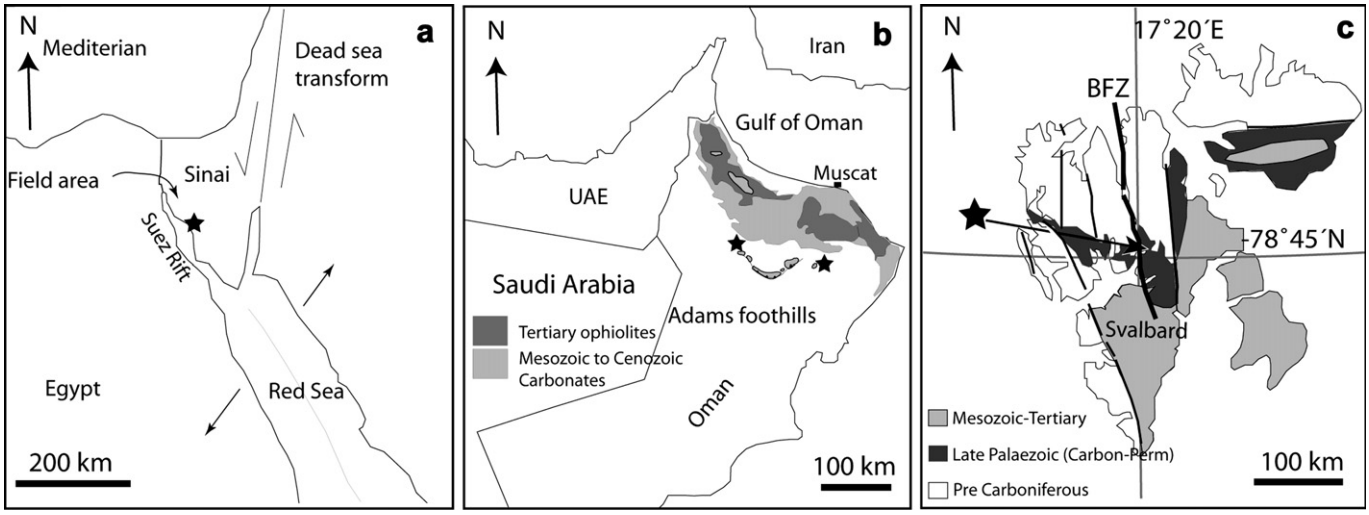

Fig. 3. a). Location of the Sinai study area (star), showing the current plate tectonic setting of the region. Arrows indicate relative plate motion. b) Tectonic map of the eastern part of the Arabian Peninsula, showing the Hajjar mountain chain and the anticline structures of the study areas of the Adams Foothills in central Oman. The Jebel Madar (east) and Jebel Quasaybah (west) study areas are denoted with stars. c) Tectonic map of the Spitsbergen island, showing large faults, including the Billefjorden fault zone (BFZ) and the map distribution of pre-Carboniferous, late Palaeozoic and Mesozoic to Tertiary bedrock units. The star locates the study area.

the Sudr, Esna, Thebes, Darat and Tanka formations (Fig. 4b). Most data points for the present study were collected from faults in the Sudr, Thebes, Darat and Tanka formations. The Thebes Formation (Said, 1960; Kuss et al., 2000) is a massive, deep water, fossiliferous limestone, characterized by abundant bands and concretions of chert and layers of marl. The formation exhibits significant lateral variation, both in composition and thickness (Moustafa and Abdeen, 1992), changing from deep marine, massive micrite horizons in the north to cherty micritic wackestone in the south (Moustafa, 2004). The unit exhibits successions of massive limestone and heterogeneous intervals of bedded chert, marl, limestones and 10–50 cm calcareous clay beds. The Thebes Formation forms a minor reservoir, cap rock and potential source to the hydrocarbon fields of the central Suez Rift (Alsharhan, 2003). The Darat Formation consists of a succession of massive chalky limestones and 0.5–2 m thick limestone beds intercalated with 1–5 cm muddy to clayey limestone and up to 0.5 m thick calcareous clay units. The Tanka Formation is a brilliantly white, bedded, chalky limestone with thin layers of flaky marl, deposited in a shallow intertidal environment. This unit is only exposed in the northern and central part of the Hammam Faraoun block, and is missing in southern parts of the region due to uplift and rift-shoulder erosion (Moustafa, 2004).

4.2. Central Oman

The study site is located in the carbonate platform of the Adams Foothills. The investigated faults are situated in the two mountain areas separated by a distance of 100 km; the Jebel Quasaybah and the Jebel Madar (Fig. 3b) (Grélaud et al., 2006). Jebel Quasaybah is located at the western end of a 70 km long, E–W oriented anticline (Fig. 3b), whereas Jebel Madar is formed by a local salt dome (Immenhauser et al., 2007). Outcrops are found in the hillsides and along valleys cutting into folded and faulted carbonates of Jurassic to Cretaceous age (Scott, 1990; Wagner, 1990). The structural configuration reflects the early Tertiary plate-scale closure of the southeastern Persian Gulf (Hanna, 1990), with major detachment folds located above blind thrusts located in Paleozoic salt layers (Al-Kindi et al., 2006). Within the major folds, there are smaller faults, distinguishable as steeply dipping normal and strike-slip faults and thrust faults. Faults are also located along the hinges of regional folds associated with salt diapir-driven flexuring (Montenat et al., 2000; Immenhauser et al., 2007).

Faults at the studied sites are hosted by early to middle Cretaceous carbonates (Grélaud et al., 2006). These can be divided into three units, from base to top: the Shuaiba, Nahr Umr, and Natih formations (Alsharhan and Nairn, 1997; Grélaud et al., 2006). The Shuaiba Formation (40–125 m thick) is characterized by massive limestones consisting of packstones and wackestone beds, whereas the Nahr Umr Formation (150 m thick) is a thick green shale section with some thin beds of micritic and marly limestones. The uppermost Natih Formation (350 m) consists of layered mudstone and wackstones/packstones (Alsharhan and Nairn, 1997).

4.3. Central Spitsbergen (Svalbard)

The dataset from Spitsbergen was collected from a rift-basin found in the inner parts of the Billefjorden area (Fig. 3c). Several phases of tectonic activity have been reported from the basin bounding master fault system, the N–S trending Billefjorden fault zone (e.g. McCann and Dallmann, 1996). Of special interest to this study is mid- to late-Carboniferous to Permian (?) extension causing the formation of the Billefjorden Trough; a more than 2000 m deep and 30–40 km wide, asymmetric rift-basin filled by mixed clastic, carbonates and evaporites (Johannessen and Steel, 1992; Maher and Braathen, in press). Syn-rift deposits are found in the Ebbadalen and Minkinfjellet formations, whereas the Wordiekammen Formation constitutes the late-rift succession. The latter unit reflects a transition to a regional, stable platform setting that prevails in Spitsbergen and the Barents Shelf (Pickard et al., 1996; Samuelsberg et al., 2003). The faults studied are formed in the late Carboniferous to Permian Wordiekammen Formation. This unit consists of 1–10 m thick micrite layers that may be subdivided into the so-called “black crags” (Pickard et al., 1996). The crags are separated by m-thick calcareous shales and wacke/packstones. The base of the Wordiekammen Formation is in many places characterized by breccia pipes known as the “Fortet Breccia Formation”. These pipes represent paleo-karst breccias formed due to collapse into cavities which were formed due to extensive karstification of

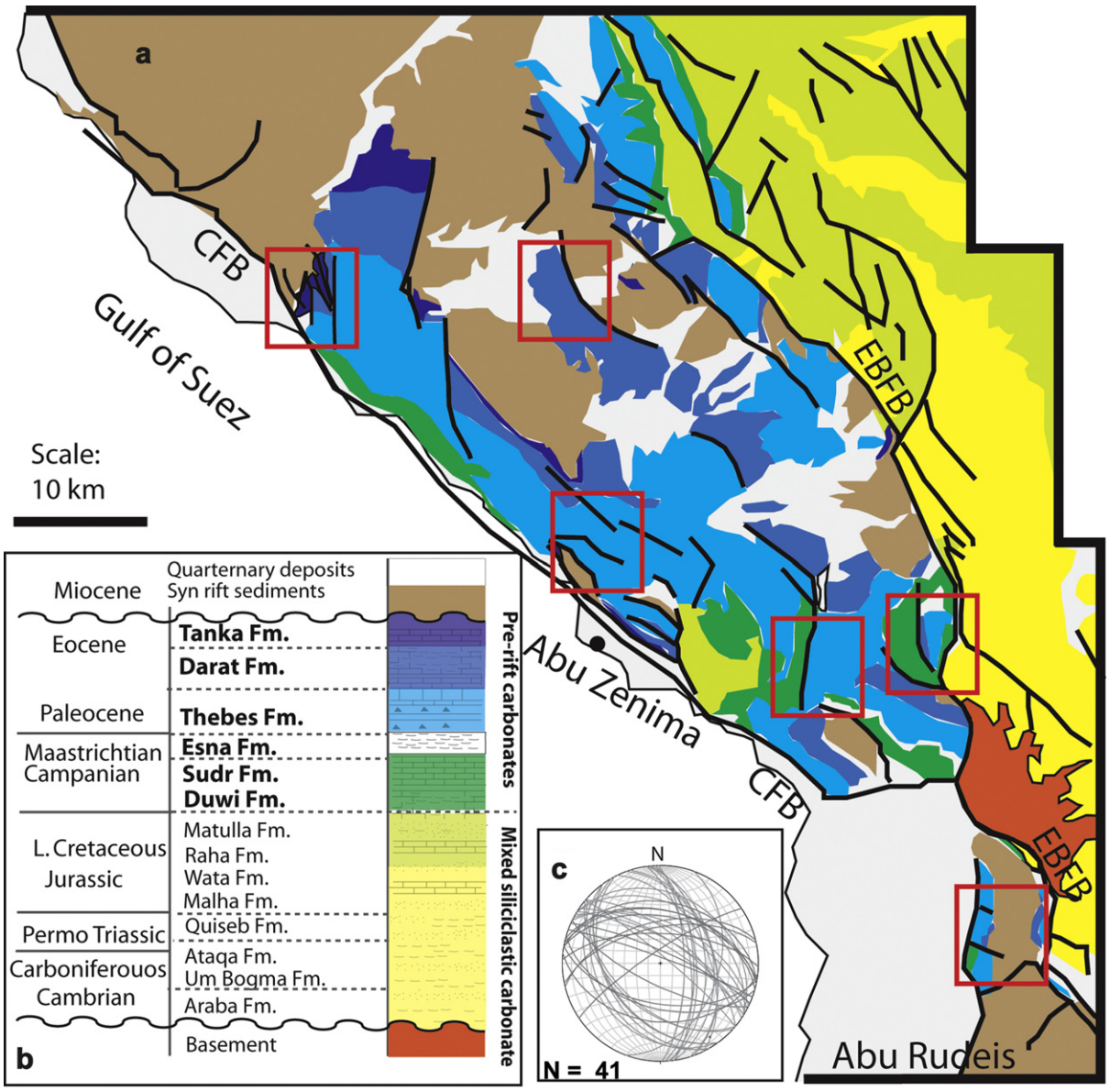

Fig. 4. a) Geological map of the Sinai field area, adopted from Moustafa (2004). Red squares indicate areas where faults have been studied. CBF – coastal fault belt, EBFB – eastern boundary fault belt. b) Simplified stratigraphical column of western Sinai, highlighting the carbonate succession of the El Egma Group. c) Stereographic plot (lower hemisphere, equal area stereo net) showing the orientation of the studied faults. (For interpretation of the references to colour in this figure legend, the reader is referred to the web version of this article).

underlying gypsum in the late Carboniferous Minkinfjellet Formation (Eliassen and Talbot, 2003).

5. Field data

5.1. Faults in Western Sinai

The majority of the studied extensional faults in western Sinai are oriented NW–SE, i.e. parallel to the regional structural grain (Fig. 4c). Some faults oriented N–S and NE–SW were also observed. Most faults juxtapose pre-rift carbonates, with a few exceptional faults that juxtapose the Tanka Formation with syn-rift sedimentary rocks. The majority of fault outcrops were observed in the Thebes and Darat formations, but some faults juxtapose the Sudr and/or Esna formations (shale) with the Thebes Formation. The limestone beds fall into two categories; 1) massive- to bedded-limestone (Thebes, Sudr and Tanka formations) and 2) interbedded limestone shale (Darat Formation). The displacement on the studied faults is listed in Table 1.

5.1.1. Small offset faults

Small faults in the massive limestone beds of Darat, Thebes, Sudr and Tanka formations have a geometry characterized by straight and slightly curved fault segments (Fig. 5a,b). Lenses and fault splays appear in breached fault overlaps and near fault bends. In most cases the fault core in these carbonates is composed of membranes of calcite veins and thin (mm) clay gouge along slip surfaces. Fault cores dominated by veins of crystalline calcite were identified as a fault core facies in approximately 70% of all studied small faults in Sinai. Most of these veins are cut by multiple fault-parallel shear fractures, and are therefore classified as sheared calcite veins. In many cases, these sheared calcite veins are associated with thin clay gouge membranes and calcite gouge membranes associated with striated slip surfaces. The latter are commonly positioned along the fault core to host rock boundary.

Table 1
Summary of fault core data from the Sinai study area. For each studied fault the displacement, maximum and minimum thicknesses, fault core composition and geometry are listed. Abbreviations are given in Fig. 1.

	Fault loc.	Displacement (cm)	Thickness (cm)	Protolith	Fm.	Fault geometry	Fault core composition
Small offset faults (>1 m)	Si1	4	0.3–0.7	Calcareous clay-limestone	Darat	1a	SCa + G
	Si2	11	0.7–3.3	Calcareous clay-limestone	Darat	1a	SCa + SS
	Si3	11	0.7–1.9	Calcareous clay-limestone	Darat	5	SCa + SS
	Si4	2.6–12	0.2–2.5	Bedded limestone	Tanka	1c&5	SCa + SS
	Si5	13	0.5–1.3	Calcareous clay-limestone	Darat	1b	SCa + SS
	Si6	14	1.5–2.8	Bedded limestone	Tanka	3a, 1c	SCa + SS
	Si7	17	2–2.4	Calcareous clay-limestone	Darat	1a	SCa + SS
	Si8	21.5	0.4–5	Calcareous clay-limestone	Darat	1a&5	SCa + SS
	Si9	4–23	1–22	Limestone-clay-chert	Darat	1b&3a	CB + G
	Si10	25	0.5–2	Bedded limestone	Tanka	1a	SCa + G
	Si11	2.6–27.3	1.3–3.25	Bedded limestone	Tanka	1c	SCa
	Si12	10–29	0.7–1.2	Calcareous clay-limestone	Darat	1a	SCa + SS
	Si13	32	1.8–3	Bedded limestone	Tanka	1a	SCa
	Si14	25–33	0.2–2.4	Calcareous clay-limestone	Tanka	4	SCa + SS
	Si15	35	0.3–1.5	Bedded limestone	Tanka	2c	SCa + G
	Si16	26–37	2.6–9.5	Calcareous clay-limestone	Darat	1b	CB + SS
	Si17	37	9–23	Bedded limestone	Tanka	3a	CB + G + SCa
	Si18	40	2.8–7.3	Bedded limestone	Tanka	1a	SCa
	Si19	3–41	0.1–1.5	Calcareous clay-limestone	Darat	2a & 5	G + SS
	Si20	38–45	0.1–0.4	Bedded limestone	Tanka	1a	G
	Si21	49	0.2–2.7	Bedded limestone	Tanka	1a	SCa + G
	Si22	40–59	1.5–13	Bedded limestone	Thebes	4	Composite
	Si23	60	1–10	Calcareous clay-limestone	Darat	1b	Composite
	Si24	53–68	0.2–10	Calcareous clay-limestone	Darat	2c & 5	SCa + SS
	Si25	75	2–4.7	Calcareous clay-limestone	Tanka	5	SCa + SS
	Si26	75	0.8–9.5	Bedded limestone	Tanka	1a	SCa
	Si27	80	1.5–9	Calcareous clay-limestone	Darat	1a	Composite
	Si28	80	2–7	Massive limestone	Thebes	3a	SCa + G
	Si29	80	0.5	Massive limestone	Thebes	1a	G
	Si30	80	1.2–6.5	Bedded limestone	Tanka	1a&5	SCa
	Si31	35–95	2.2–4.5	Calcareous clay-limestone	Tanka	1a&2a	SCa + SS
	Si32	95	0.4–7	Calcareous clay-limestone	Thebes	1b	Composite
Moderate offset faults (1 m–10 m)	Si33	100	1.3–12	Bedded limestone	Tanka	1b	CB + SCa
	Si34	105	2.9–13	Bedded limestone	Tanka	1a&5	SCa + SS
	Si35	68–109	2.5–12	Calcareous clay-limestone	Thebes	1a&5	SS + Composite
	Si36	3–114	0.2–13.1	Calcareous clay-limestone	Tanka	4	SCa + SS
	Si37	115	2–13	Massive limestone	Thebes	5	CB + SCa
	Si38	70–135	0.1–14	Calcareous clay-limestone	Darat	2a & 5	CB + SCa + SS
	Si39	120–140	1–15	Shale-limestone	Darat	1a	Composite
	Si40	140	3–5	Bedded limestone	Tanka	1b	CB + SS + Composite
	Si41	100–150	2–6	Shale-limestone	Darat	2a	SS
	Si42	150	0.8–10	Massive limestone	Thebes	1c, 5	G
	Si43	150	0.1–6	Massive limestone	Thebes	4	Sca + G
	Si44	150	1.8–5.1	Bedded limestone	Tanka	2a&2b	Sca + G
	Si45	190	2.3–5.8	Calcareous clay-limestone	Darat	1a	SCa + SS
	Si46	200	1.1–1.4	Massive limestone	Thebes	2c	G
	Si47	220	1.3–13	Massive limestone	Thebes	1a	Sea
	Si48	250	0.2–6	Massive limestone	Thebes	1a	CB + G
	Si49	250	2.6–11.5	Bedded limestone	Tanka	1a	SCa + SS
	Si50	100–260	0.6–55	Calcareous clay-limestone	Darat	2c & 5	SCa + SS + G
	Si51	150–280	3–50	Massive limestone	Thebes	3b	CFR
	Si52	350	2–7	Limestone-clay-chert	Thebes	2b & 5	CB + SCa + G
	Si53	400	2–9.9	Shale-limestone	Darat	1a	SS + Composite
	Si54	450	5–50	Calcareous clay-limestone	Darat	5	CB + Composite
	Si55	450–500	4.5–7.8	Bedded limestone	Darat	1a	Composite
	Si56	560	1.3–27	Massive limestone	Thebes	2b & 5	CB + SCa + G
	Si57	600	10–25	Limestone-clay-chert	Thebes	5	Composite
	Si58	600	10.4	Shale-limestone	Darat	1a	SS
Large offset faults (<10 m)	Si59	1000	6–28.6	Bedded limestone	Tanka	1a&5	CB + SCa
	Si60	1600	1.4–15	Massive limestone	Thebes	5,2a	CB + G
	Si61	2800	15–20	Limestone-clay-chert	Thebes	1a	Composite
	Si62	3000	1–38	Limestone-clay-chert	Thebes	1a, 5	CB + SCa + G
	Si63	3500	4–30	Massive limestone	Thebes	5	CB + SCa
	Si64	5000	21–23	Limestone-clay-chert	Thebes	5	CB
	Si65	23 000	70–195	Limestone-chalk-shale	Sudr-Thebes	7	CB + Composite
	Si66	25 000	15–110	Bedded limestone	Tanka	7	CB
	Si67	35 000	1100	Shale (Esna)	Sudr -Thebes	7	SS
	Si68	40 000	100–490	Limestone shale	Tanka-Thebes	7	CB + SS

Calcite vein membranes are generally fairly continuous along the fault core. Their thickness varies from 0.5 to 13 cm, with the largest thickness related to fault bends where lens shaped vein bodies are formed. In most of these lenses the vein lamination curves similar to the lens shape, and the central part of the calcite filled lens exhibits open voids with sparry calcite.

In thin section, sheared calcite veins are seemed to consist of a matrix of crystalline calcite cross-cut by fractures that, in some

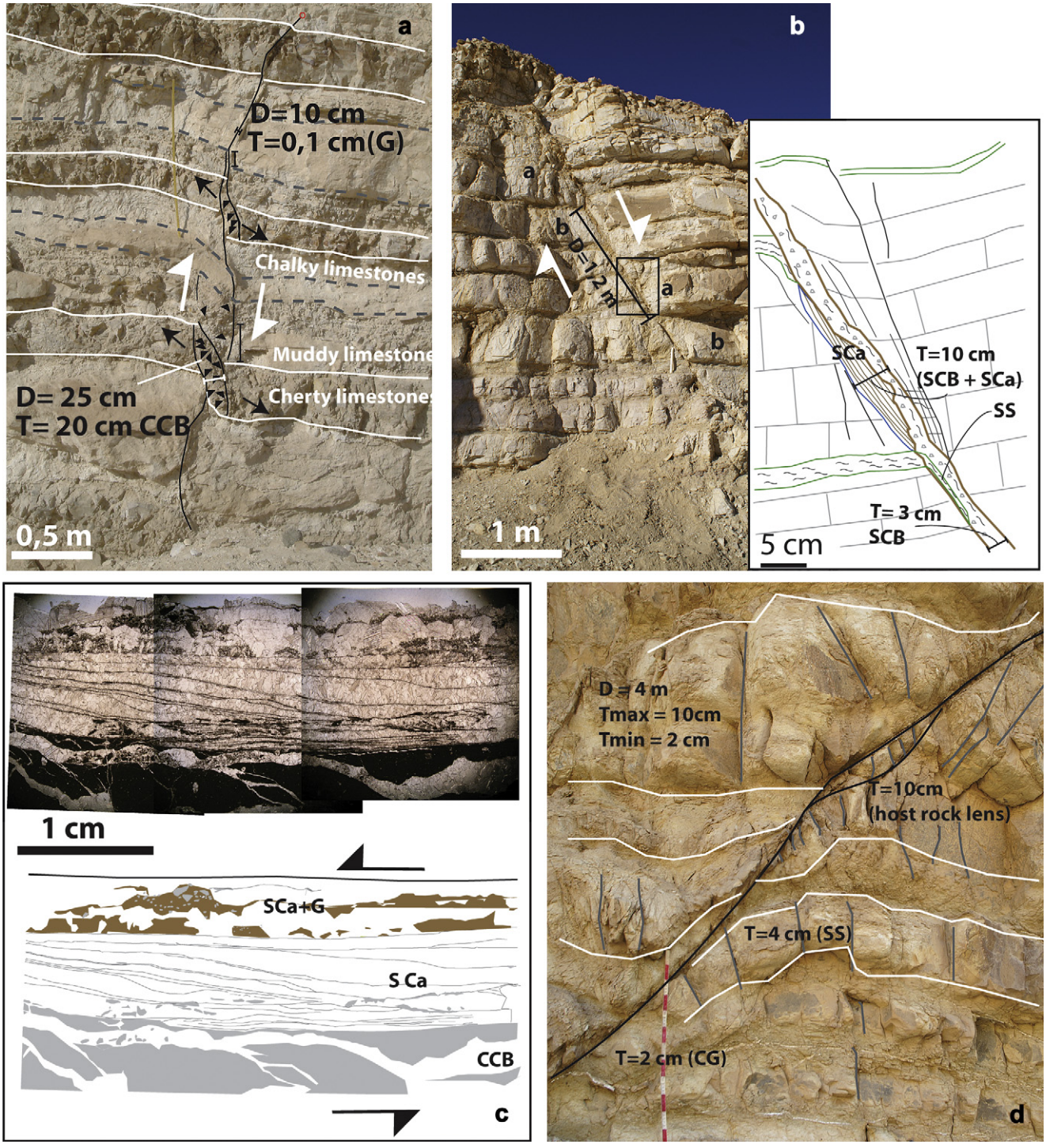

Fig. 5. Examples of small and moderate offset faults observed in Sinai, Egypt. a) Fault with 20 cm displacement hosted in marly limestone, chert and chalk layers (Thebes Formation). The fault has jogs, which are characterized by thick breccia pods next to chert layers. Thin slip zones characterize more planar parts of the fault in the limestone layers. b) Fault with 1.5 m displacement showing a fault core of calcite veins (SCa) and shale supported carbonate breccia (SCB). c) Mosaic of photomicrographs that displays the microstructures of a sheared calcite vein collected from a fault with ~2 m displacement. The upper part is a cemented gouge (SCa + G), neighbouring a zone of calcite crystals (SCa) cut by numerous curved fractures (slip surfaces). The fractures are associated with thin slivers of gouge and protolith rock, probably derived from shearing along the vein-protolith contact. The lowermost part is a cemented carbonate breccia (CCB). d) Fault with 4 m displacement cutting through marl and shale prone parts of the Darat Formation. The fault has a prominent slip surface with well developed shale smears (SS), gouge (G) and breccia (CB) membranes. Note lens formation near the fault bend and the drag of layering in the footwall and hanging wall.

cases, are coated with a thin (~1 mm) membrane of gouge (Fig. 5c). Inside the crystalline calcite vein, <1 mm thin lenses/slivers of host rock limestone can be observed.

Carbonate breccias are commonly found in lenses and typically consist of coarse, clast-supported breccia that shows extensive calcite cementation. These lenses are especially common near fault bends related to chert bands of the Thebes Formation (Fig. 5a).

In shale prone carbonates (Darat and parts of Thebes formations), small faults appear as bifurcated, splayed and bended (Fig. 5a). In these faults, lenses occur as partly shattered limestones that commonly are found along complex fault overlap zones. Shale smears, together with fault rocks lenses and calcite veins, locally form composite fault cores. The shale smears show variable smearing potential, depending on the thickness of the shale protoliths. Shale smear factors (Lindsay et al., 1993) are typically around 4.

5.1.2. Moderate offset faults

In faults with moderate offset, calcite veins occur as broken up lenses and/or juxtaposed with other fault core facies, such as breccias and shale smears (Fig. 5b,d). Carbonate breccias are more common compared to small faults, constituting 35% of the core facies. The breccia matrix mostly consists of calcite gouge that is cemented, but in the shale prone units breccias are also shale supported. The carbonate breccias are arranged in semi-continuous membranes or as highly elongated lenses, bound by slip zones, often in association with shale smears and calcite veins.

5.1.3. Large offset faults

Faults featuring 10–50 m displacements were only observed in the massive parts of the Thebes Formation. These are characterized by relatively thin fault cores (2–50 cm) consisting of membranes of fine grained (sub-mm clast size) carbonate gouge/breccias, thin clay gouge, calcite veins and fault rock lenses (Fig. 6a). The lenses are 2–5 m long and may be 20–50 cm thick, consisting of fine grained to coarse grained breccias.

In large faults with more than 100 m displacement, shale smears of the approximately 50 m thick Esna and Thal formations (between Darat and Tanka formations) are common (Fig. 6b,c). These faults may be totally dominated by shale smear, and the thickness of observed shale layers in cores are up to 11 m in large faults juxtaposing the upper Sudr to the Darat formations. However, common thicknesses are around 0.5–3 m. In some cases these shale smears are associated with thick layers of coarse grained fault breccias, partly shattered limestone and calcite veins along slip surfaces. They are classified as composite fault cores (Fig. 6b). In larger faults or in positions far away from the source shale layer of the Esna shale, the displacement exceeds the smearing potential of the shale. Fault cores in these cases are dominated by breccia membranes and thin and patchy lenses/pockets of shale (Fig. 6c). All large faults are accompanied by a well-defined damage zone consisting of fractures, small and partly moderate faults, and, locally stylolites.

5.2. Faults in central Oman

Faults studied at the Jebel Madar locality are mostly N–S and NE–SW oriented, steep and defining horst-and-graben structures parallel to the salt diapir fold crests (Fig. 7a,b). In this locality the displacement of the studied faults varies between 10 cm and 300 m, but may be much larger in other parts of the Jebel Madar (Fig. 7a and Table 2a). In the Jebel Quasaybah area, data were collected from an array of extensional faults, dipping 60°–80°, bounding N–S trending narrow graben structures. These faults are found in well bedded Natih Formation units (Fig. 7b). The range of displacements range from this area is between 10 cm and 50 m. Similar to the Sinai faults, geometry and compositional characteristics vary as a function of the

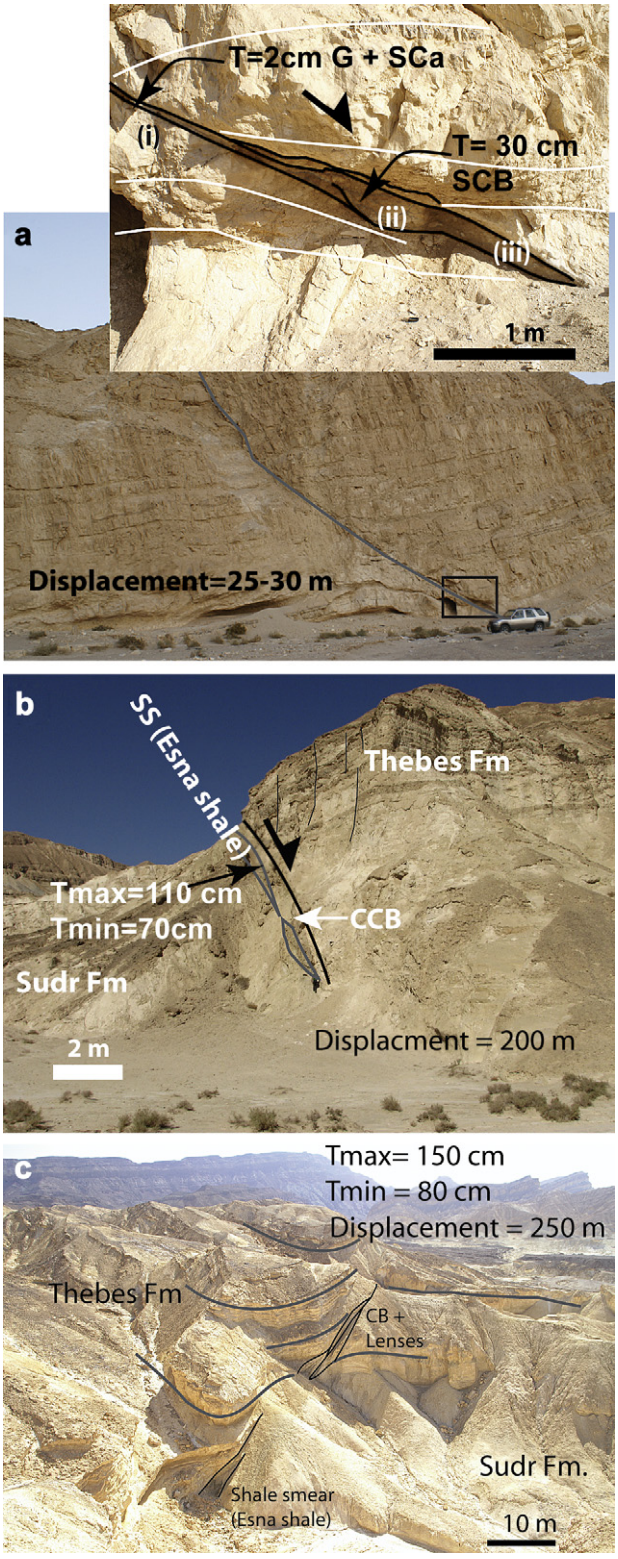

Fig. 6. a) Photograph of fault with ca. 25 m displacement hosted in the Thebes Formation. The fault is oriented NW–SE and dips towards the SW. Details of the fault core are: (i) Localized fault core with secondary calcite veins and gouge, (ii) distributed slip zones bounding a protolith lens, and (iii) carbonate fault rock lens. b) Large (~200 m displacement) fault juxtaposing the Thebes and Sudr formations. The fault core has two main elements; shale smear layers derived from the Esna shale and layers of cemented breccias derived from limestones and cherts of the Thebes Formation. c) Large fault (~250 m displacement) juxtaposing the Thebes Formation with the Sudr Formation. The upper part of the exposure is characterized by fault slip zones bounding lenses of carbonate breccia and host rock. The lower part consists of shale smear derived from the Esna Formation.

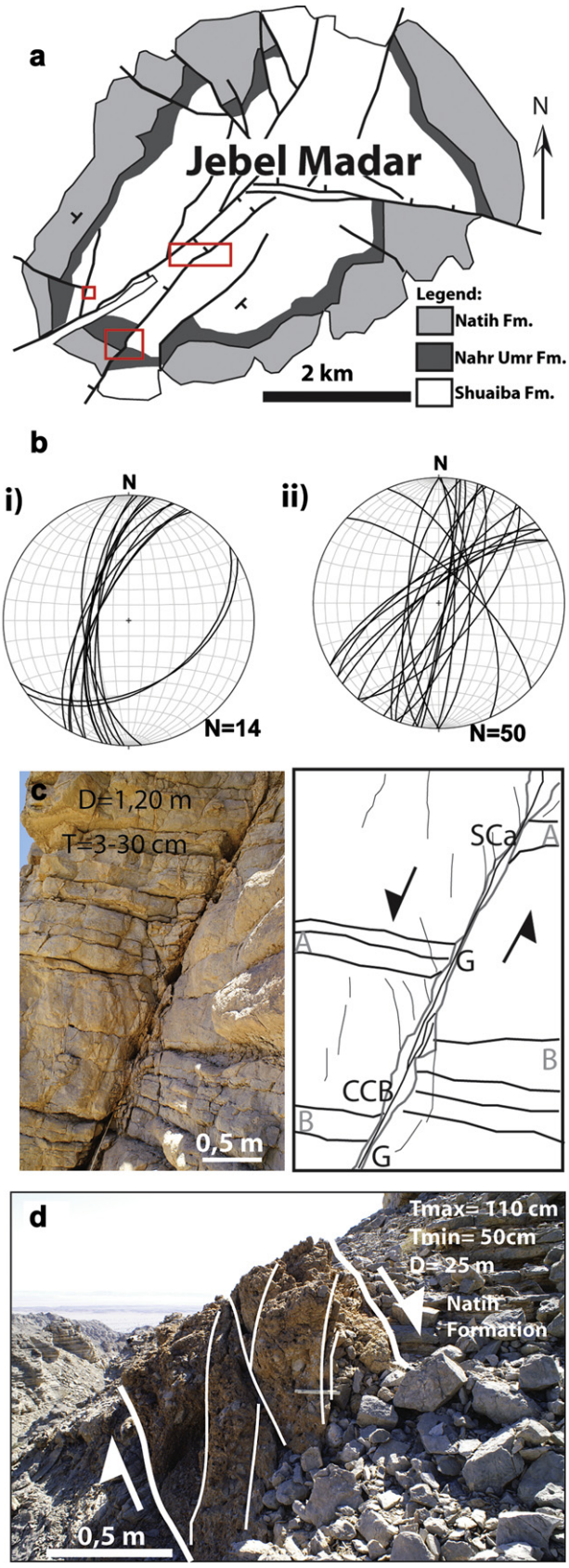

Fig. 7. a) Map of the Jebel Madar area modified from Immenhauser et al. (2007). The Jebel Madar forms a dome shaped anticline, with associated extensional faults. The studied localities are indicated by boxes. b) Stereo plots of faults studied in the Jebel Quasaybah (i) and Jebel Madar (ii) localities, showing a steep N–S orientation of the faults. c) Fault from the Jebel Madar with 1.20 m displacement hosted in the Shuaiba Formation. The fault core is dominated by irregular secondary calcite veins and patches of cemented carbonate breccia and gouge. d) Fault with approximately 25 m displacement hosted in well bedded Natih Formation at the Jebel Quasaybah site. The fault core consists of a thick layer of well cemented carbonate breccias, there is a fine grained breccia close to the footwall, grading into a coarse grained proto-breccia towards the hanging wall.

protolith carbonate rock. For example, the mud-rich carbonates of Natih Formation (in Jebel Madar), exhibit faults with thin and localized fault cores. The faults typically feature a curved and well-defined slip surface, similar to some of the thin, large faults in the massive parts of Thebes Formation of Sinai. In contrast, faults in the massive and stiff limestone layers of the Shuaibah Formation exclusively host fault cores of massive thick membranes of cemented breccias and/or sheared calcite veins. Shale smear is not observed to the same degree as in the faults of Sinai.

5.2.1. Small and moderate offset faults

Calcite precipitations dominate small faults observed in the Shuaibah and Natih formations of Jebel Qusaybah. They are characterized by sheared veins similar to those studied in Sinai. Carbonate breccias are formed as discontinuous lenses in small faults (Fig. 7c) and form semi-continuous membranes in faults with more than 2 m displacement. At the Jebel Qusaybah site, the moderate offset faults are composed of coarse breccias. Typically, limestone breccia clasts are separated by a pattern of conjugated Riedel and anti Riedel veins of red/brown coloured calcite (Fig. 7d). Fault cores with this pattern are characterized by a gradual transition from fault core to damage zone, without any clear slip surface boundary. Conversely, in the Natih Formation of the Jebel Madar site, moderate to large offset faults appear as narrow zones consisting of discrete slip surfaces associated with a thin fault gouge, and are rarely associated with calcite precipitations. Carbonate breccias are commonly discontinuously distributed as lenses or pockets along the fault core margins.

5.2.2. Large offset faults

With increasing slip, the fault cores of the large faults of Jebel Quasaybah are associated with several slip surfaces bounding units of fine grained breccias embedded in coarse grained breccias of red/brown calcite (Fig. 7d). Typically, fine grained breccias appear along slip surfaces towards the footwall. A second type of large offset fault consists entirely of slip surfaces hosting crystalline calcite veins. These fault cores are observed in the Jebel Madar site and have thicknesses ranging from 50 to 300 cm. And some veins extend for approximately 100 m in strike direction. The calcite veins are sheared by numerous parallel and corrugated slip surfaces. This shearing causes a compartmentalization of sheets with different calcite textures, from fine grained crushed and brecciated calcite to large undeformed blocky and acicular crystals that can be 30 cm in length. The blocky crystals are oriented perpendicular to the slip surfaces, and grow into fault-parallel voids, whereas acicular crystals exhibit radial growth directions, initiating from protolith clasts. The slip zones are characterized by sub-mm gouge membranes and thicker zones consisting entirely of crystalline calcite breccias.

5.3. Faults in Central Spitsbergen

The majority of faults are observed in intact, but highly fractured and semi-brecciated limestone of the Wordiekammen Formation and Fortet Breccia member. Pressure solution contacts are seen in both lithologies, indicating a deeper maximum burial of the rocks, in contrasts to the Sinai and Oman areas. This is expected since the rocks are older and have undergone several burial and un-roofing events (Steel and Worsley, 1984; Maher and Braathen, in press).

Table 2
Summary of fault core data from the Oman (A) and Spitsbergen (B) study areas. For each studied fault the displacement, maximum and minimum thicknesses, and fault core characteristics are listed. Abbreviations are as follows; G-gouge membrane; SCa-secondary calcite; CFR-carbonate fault rock; SS-shale smear.

	Displacement (cm)	Thickness (cm)	Protolith	Fault geometry	Fault core composition
Oman					
Om1	18	13–22	Bedded limestone	3b	SCa
Om2	40	18	Bedded limestone	1c	SCa
Om3	70	5–13.5	Bedded limestone	1a	SCa
Om4	70	2–10	Bedded limestone	3a	CB
Om5	100	20	Bedded limestone	1b	SCa
Om6	100	10	Bedded limestone	1c	CB
Om7	100–130	5–38	Bedded limestone	1b&5	CB + SCa + G
Om8	150	12–40	Bedded limestone	3a	CB
Om9	300	20–25	Bedded limestone	1a	SCa + SS
Om10	300	13–35	Bedded limestone	1a	CB
Om11	100–350	12–23	Bedded limestone	2a	SCa
Om12	400	2–40	Bedded limestone	2c	CB
Om13	630	21–29	Bedded limestone	2b	SCa
Om14	1000	15–25	Bedded limestone	1a	SCa + CB
Om15	1000	100–110	Bedded limestone	2c	CB
Om16	1500	2–16	Bedded limestone	1a	CB + G
Om17	1800	160–180	Bedded limestone	2c	CB
Om18	2000	170–200	Bedded limestone	7	CB
Om19	2000	75	Bedded limestone	7	CB
Om20	4200	150–170	Bedded limestone	7	CB
Om21	11 500	70–200	Bedded limestone	7	CB + SCa
Om22	28 800	400	Bedded limestone	7	CB
Spitsbergen					
Sv1	15	6–9	Limestone shale	4&5	CB
Sv2	17	0.1–1.1	Limestone shale	1a	CB + G
Sv3	22	5–8	Limestone shale	4	CB
Sv4	34	0.5–15	Limestone shale	1a	CB + SCa
Sv5	45	0.6–13	Limestone shale	4&2a,1b	CB
Sv6	50	0.5–8	Limestone shale	2c & 4	CB + G
Sv7	80	2–4	Limestone shale	4	CB
Sv8	100	17	Breccia pipe	2a	CB
Sv9	130	80	Breccia pipe	2a	CB
Sv10	135	0.3–17	Limestone shale	4&5	CB + G
Sv11	400	0.3–40	Breccia pipe	5&1a	CB + G
Sv12	540	7.5–59	Limestone shale	5&1a	CB + G
Sv13	20 000	350	Collapse breccia and limestone	7	CB + G

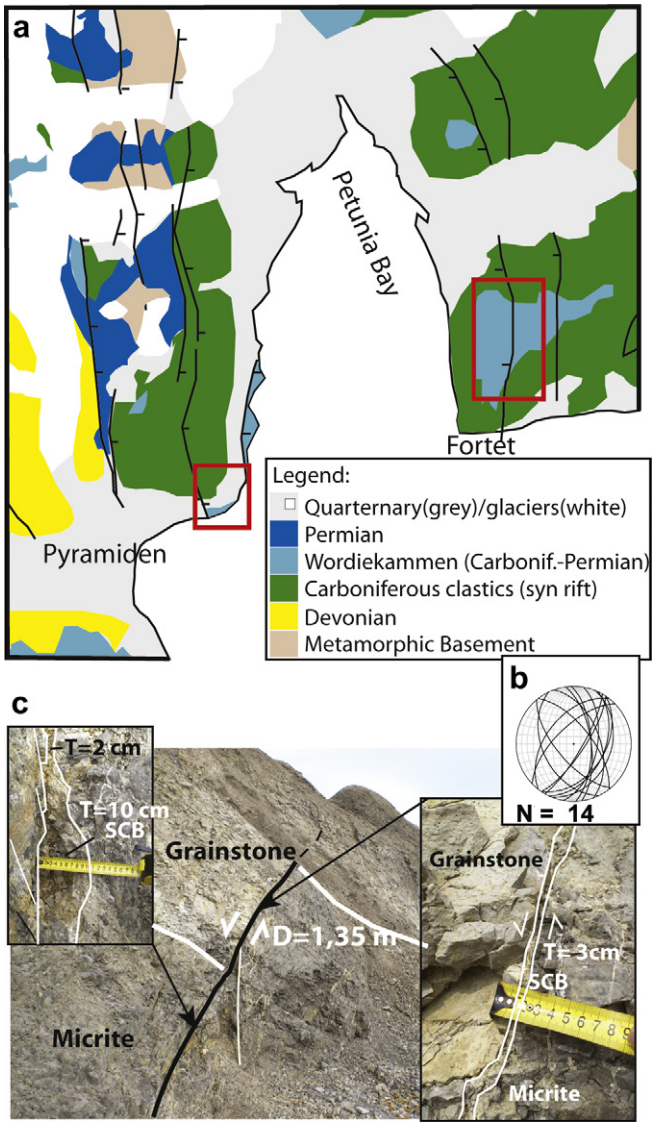

Fig. 8. Field localities from the Central Spitsbergen area. a) Geological map of the inner Billefjorden area, with a simplified stratigraphic legend. b) Stereographic plot of orientation of faults studied in Billefjorden, indicating a general N–S trend parallel to the regional grain. c) Fault with 1.35 m displacement that juxtaposes a fossiliferous grainstone with a micrite. The measuring stick is 1 m. The left inset photograph shows a complex fault core composed of thick shale supported breccia and gouge membranes. The right inset photograph shows a localized fault core within a restraining bend. The fault core is here a thin membrane consisting of a fine grained shale supported carbonate breccia (SCB).

The dataset covers faults trending NW–SE, N–S and NE–SW, which is parallel to the local and/or regional structural grain (Fig. 8a,b). The faults are located near Pyramiden and at Fortet, which both host karst breccias. At the Pyramiden site, one master fault (major segment within the Billefjorden fault zone) cuts through the entire Wordiekammen Formation, and stratigraphic correlation suggests a throw exceeding 250 m. Of the 13 faults studied, most reveal geometries of overlapping and breached segments, fault splays and lenses (Table 2b).

5.3.1. Small and moderate offset faults

In contrast to the faults in Sinai and Oman, the small faults in Spitsbergen exhibit breccias and generally lack the extensive calcite veins. The overall observation is steep, localized fault cores consisting of carbonate breccias, with a jagged boundary towards a densely fractured (jointed) carbonate host rock. The fault orientation and core geometry seem well connected with the orientation of joints. Fault breccias are mostly shale supported, but bordered by a thin membrane of clay gouge (Fig. 8c). In some cases there are cemented coarse grained breccias bound by striated slip surfaces. Stylolites are localized to the contact between breccia clasts, consistent with local pressure solution and calcite precipitation in breccias. The bulk of the dataset shows fault core thickness variations ranging from 0.1 to 15 cm.

5.3.2. Large offset faults

The outcrop of the master fault at the Pyramiden site (250–300 m displacement) reveals a fault core and a hanging wall damage zone comprising a 60 m wide zone of brecciated and intensively fractured limestone. Bedding in both the footwall and hanging wall dips 20°–40° towards the southeast, increasing towards the fault core, indicating a normal drag towards the fault. Extensional faults observed in the damage zone of the hanging wall are therefore assumed to be rotated, in that extensional faulting took place prior to or during folding; many of these faults are described in the small to moderate offset fault section above. The core thickness of this large fault is approximately 3.5 m. It consists of a matrix-supported breccia with limestone clasts of 0.1–1 cm, cut by numerous slip surfaces with mm-thick gouge membranes.

6. Facies and thickness–displacement analysis

In this section we summarize the distribution of fault facies for the faults found in carbonate rocks of the three study areas. We then evaluate the thickness/displacement relationships. Finally, we compare the combined relationships between thickness/displacement vs. geometry and composition.

6.1. Facies analysis

6.1.1. Composition

Of all the fault cores, regardless of field area and displacement, 34% consist of carbonate breccias, 22% are composed of shale smears and 20% consist of sheared cement veins. Furthermore, 20% of the cores have a combination of all the above mentioned elements (composite core) (Fig. 9a). Only 5% of the faults consist of gouge; however this element is commonly a minor volumetric constituent in fault cores dominated by calcite veins or by slip surfaces in larger faults. Separating the data into different fault scales reveals that there is a gradual change of fault core facies from small to large faults.

In the *small faults* the most common facies combination is that of calcite veins and gouge (30%). Combinations of calcite veins and shale smear are also common occupying 28% of the dataset, whereas fault cores dominated by breccias constitute 21%.

In *moderate offset* faults a mixture of compositional elements, such as smeared shale layers, cemented breccias and veins of calcite, become more common (28%). Also, shale smear is more frequent, probably related to more prominent thicker shale layers that are dragged along faults. Furthermore, the calcite veins become less apparent (13%) and carbonates breccias (35%) become more common.

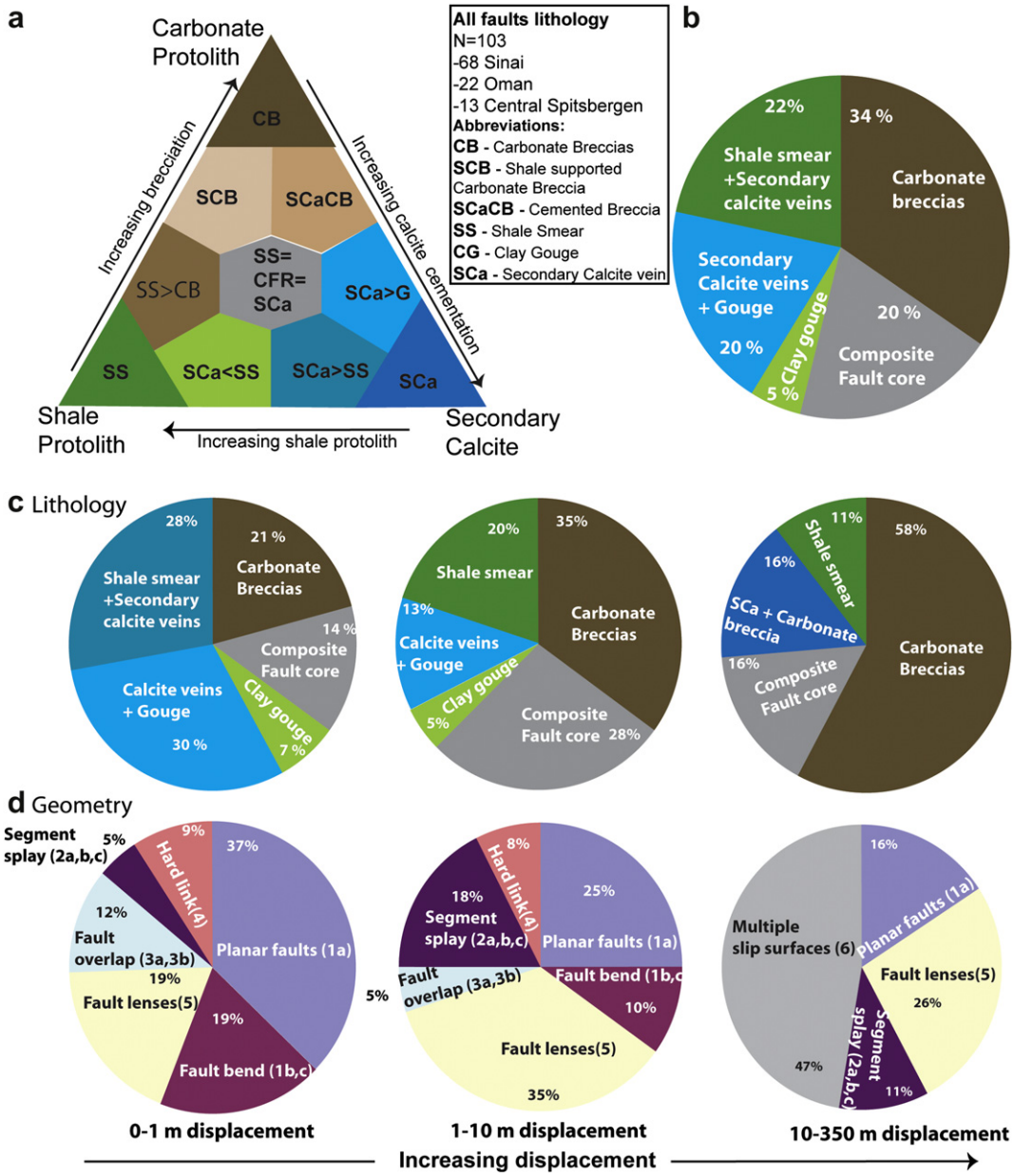

Fig. 9. Facies distribution of fault core lithologies and geometries divided into displacement intervals. a) Lithological facies diagram similar to the classes of Fig. 1. with colour coding b) Pie chart displaying the composition of all faults studied. c) and d) Pie charts displaying the percentage of compositional and geometrical facies for fault offset ranges of 0–1 m, 1–10 m, and 10–400 m.

For *large faults*, breccias are the most common constituent occupying 58%. There are fewer fault cores with only shale smear (11%); however, many of the faults with composite facies elements (16%) have a significant part consisting of shale. Cores with calcite veins in combination with carbonate breccia occupy 16% of the composition of this displacement range.

6.1.2. Geometry

The analysed dataset shows 30% planar fault segments, i.e. segments without complexities (Fig. 9b). On the other hand, 70% of the faults show complexities, ranging from fault splays, to lenses and to multiple arrays of slip surfaces. Most of the planar fault segments are found for small faults (37%), whereas this geometry decreases with increasing displacement, constituting 25% for moderate offset faults, and 16% of the large faults. The largest fault with a planar geometry has 50 m displacement. Fault lenses are observed in 20% of the small faults, whereas for moderate offset faults lenses comprise 35% of the dataset. In large faults, lenses again become less common. For large faults, nearly 50% of the cores show multiple slip surfaces, which corresponds to the entire dataset of faults with more than 100 m displacement.

6.2. Thickness–displacement relationships

From the 103 faults, 423 thickness measurements were made. Out of these, 334 are from Sinai, 58 from Oman and 31 from Svalbard (Fig. 10). The displacement along the observed faults ranges from 4 cm to 400 m, of which the majority (80%) of the faults exhibit displacements below 10 m. Of these, a significant number (40%) have displacements of less than 1 m (Fig. 10a). The thickness of the fault cores increases with increasing displacement; for displacement below 1 m the fault cores display thicknesses between 0.1 cm and 23 cm, for moderate offset faults the thickness varies between 0.1 cm and 55 cm, and for large faults the thickness varies between 1 cm and 11 m. For faults with more than 200 m of displacement, the minimum thickness is 50 cm, and thicknesses above 3 m are always related to smearing of major shale layers.

The thickness/displacement relationship of all fault core measurements shows that there is a positive correlation between thickness and displacement with a linear correlation of $0.01 \times D + 0.067$ (Fig. 10b). This trend is validated by a regression value of $R^2 = 0.45$. For the same dataset, a power law line can be calculated ($aX^b = 0.29D^{0.56}$), where a 95% prediction belt indicates a scatter covering more than three orders of thickness values. Regression value (R^2) for the power law line is 0.44. The exponent of 0.56 for the power law equation is consistent with smaller faults having a relatively high thickness–displacement ratio, with a gradual decrease in this ratio for larger faults. In more detail, the average plots of the thickness–displacement (T/D) relationship for each of the studied fault scales show a decrease from D/32 of small faults with an average of 40 cm displacement, to D/81 for moderate offset faults with an average of 2.3 m displacement, and to D/267 for large faults with an average of 79 m displacement (Fig. 10c).

6.3. Facies combinations and thickness/displacement relationship

By combining the thickness/displacement data with the compositional and geometrical information we can go deeper into the fault core characteristics (Fig. 11 and Table 3). In this analysis we use arithmetic graphs to further investigate the relationship between thickness/displacement and facies. These graphs are divided into small (Fig. 11a,b), moderate (Fig. 11c,d) and large offset faults (Fig. 11e,f). The combination of geometrical and compositional facies is then compared (Table 3), for example by the average thickness value for each displacement range that represents a reference value.

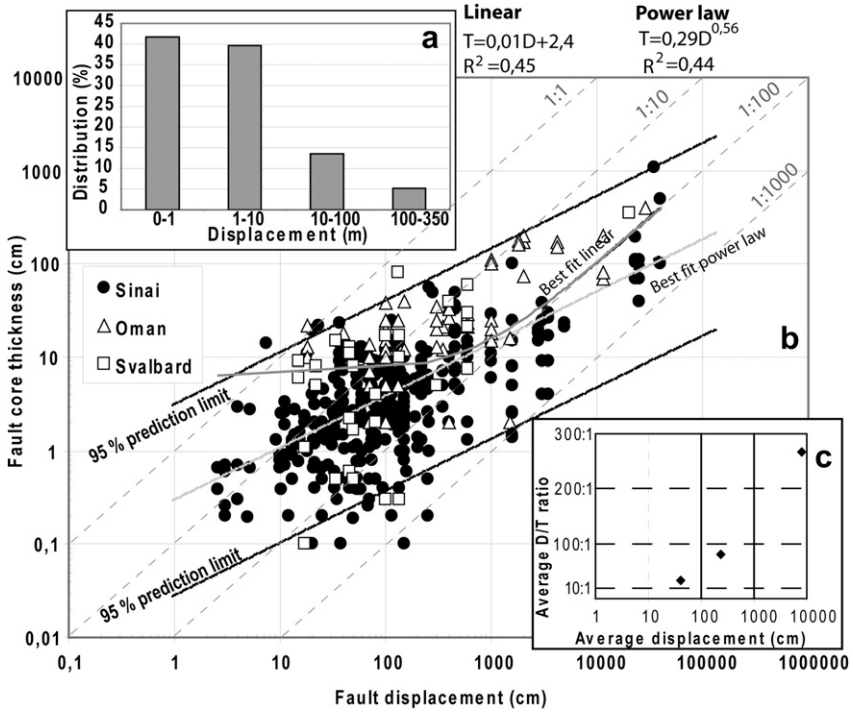

Fig. 10. Displacement vs. thickness data from the three study areas. A) Histogram showing the distribution of the displacement in intervals covering all the analysed faults. B) Thickness–displacement diagram with logarithmic axes. Dashed lines illustrate orders of thickness/displacement relationships. The regression lines are displaying the 95% prediction belt with basis in the best fit power law trend line. Note that the confidence belt shows a scatter of data over three orders of magnitude for any given displacement. C) Average displacement against average thickness to displacement ratio of three displacement ranges (0–100, 100–1000, 1000–40000 cm). This plot suggests that there is a gradual decrease in thickness to displacement ratio for increasing displacement.

Faults with thickness values above the average are termed thick faults, whereas faults with values below are termed localized faults.

For the *small faults* (Fig. 11a,b) in the range of 4 cm–100 cm displacement, there is a poor correlation between the thickness and the displacement, as indicated by the high scatter in data points (Fig. 11a). The thickness range is from 1 mm to 23 cm. There is also large variability of geometrical and compositional facies. However, combinations such as planar faults with calcite veins and gouge are far more frequent (79%) in the localized faults (thickness below 3.8 cm) than any other combination. For thick fault cores (above the average thickness of 3.8 cm) the dominant facies combinations are carbonate breccias and calcite veins located to releasing bends, and fault splays often having a lens shape. Thick planar cores are dominated by smears of relatively thick shale layers and significant accumulations of calcite veins.

Moderate offset faults (Fig. 11c,d) ranges in thickness from 1 mm to 80 cm with an average of 11 cm. The thickness distribution is skewed towards lower displacements, and there is an overall poor correlation in the relationship between thickness and displacement. Localized faults consist most commonly of planar segments

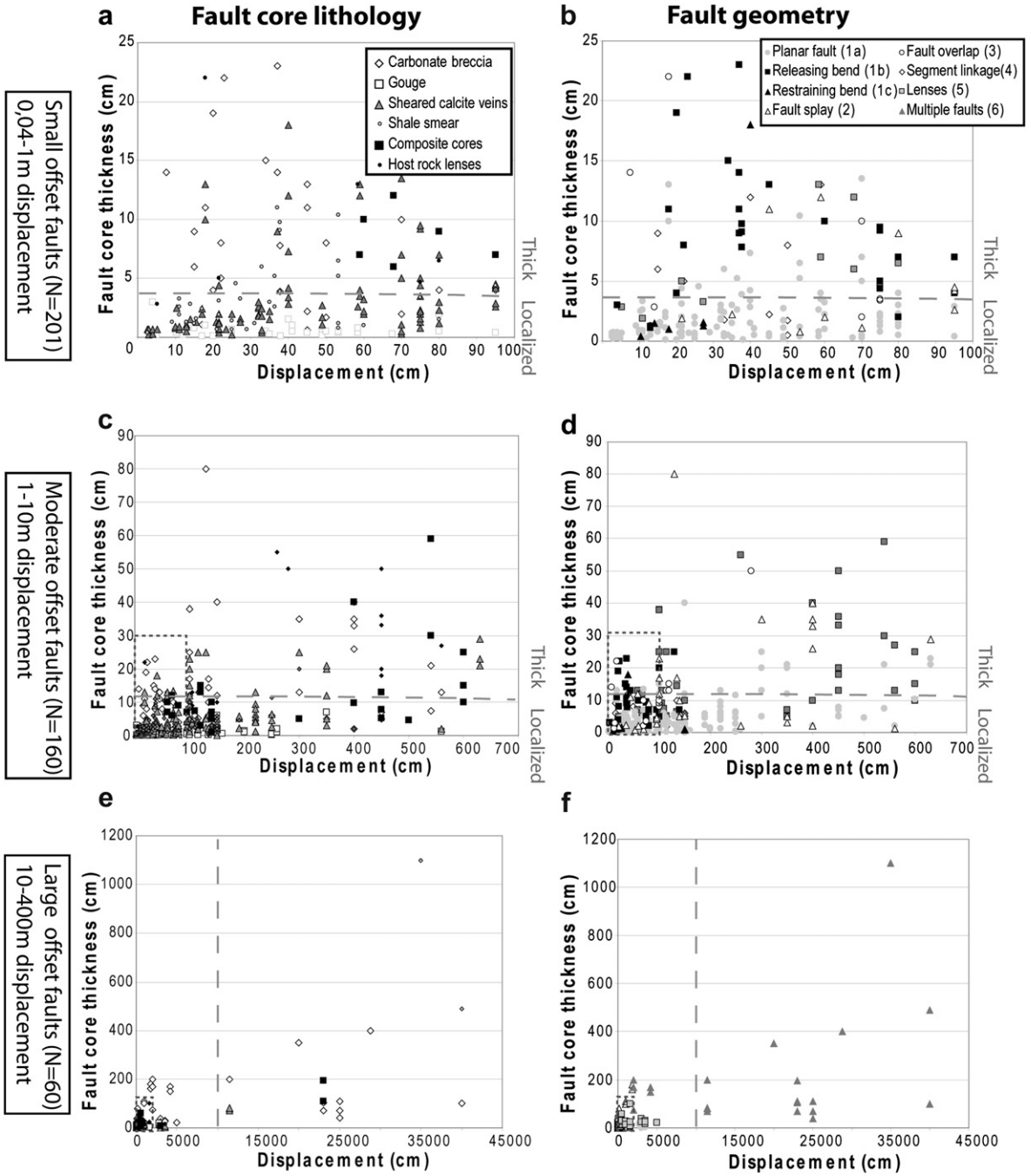

Fig. 11. A) Arithmetic displacement vs. thickness plotted using the same data points as shown in Fig. 10. The points are denoted with the lithological and geometrical characteristics, as observed in outcrops. For analysis purposes the plots are divided into small (a,b) (0–1 m), moderate (c,d) (1–10 m) and large offset (e,f) (10–400 m) faults. Dashed lines in the four lower plots indicate the level of average thickness and the transition between planar localized fault cores and thick complex fault cores. For further description see the text.

Table 3
Table showing the combination of geometrical and compositional data of all the measured thickness points. The data is shown in the plots of Fig. 11, where the thickness/displacement data is divided into small, moderate and large offset faults. The small faults have an average thickness of 3.8 cm; faults thicker than this are termed thick faults, while faults with lower thicknesses are termed localized faults. The same principle is used for the moderate offset faults, where the average is 11 cm. Few measurements from large faults make discrimination between localized and thick cores uncertain. Instead this group is divided into faults of 10–100 m displacement and faults of 100–400 m displacement.

		N	%			*N*	%
Small offset faults (*N* = 201)							
Localized fault cores (*T* < 3.8 cm)				**Thick fault cores (*T* > 3.8 cm)**			
Planar	Breccia	3	2%	Planar	Breccia	2	4%
Planar	Gouge	26	19%	Planar	Cement veins	9	18%
Planar	Cement veins	61	45%	Planar	Shale smear	6	12%
Planar	Shale smear	20	15%	Releasing bend	Breccia	11	22%
Releasing bend	Gouge	2	1%	Releasing bend	Gouge	1	2%
Releasing bend	Shale smear	1	1%	Releasing bend	Cement veins	6	12%
Releasing bend	Cement veins	1	1%	Releasing bend	Shale smear	2	4%
Restraining bend	Gouge	2	1%	Releasing bend	Composite	2	4%
Restraining bend	Cement veins	3	2%	Restraining bend	Cement veins	1	2%
Fault splay	Cement veins	4	3%	Fault splay	Breccia	1	2%
Fault splay	Shale smear	2	1%	Fault splay	Cement veins	4	8%
Overlap	Breccia	1	1%	Fault splay	Shale smear	1	2%
Overlap	Cement veins	1	1%	Overlap	Breccia	2	4%
Overlap	Shale smear	3	2%	Overlap	Lenses	1	2%
Segment link	Breccia	2	1%				
Segment link	Gouge	1	1%				
Segment link	Cement veins	1	1%				
Lenses	Shale smear	2	1%				
Lenses	Composite	1	1%				
Moderate offset faults (*N* = 160)							
Localized fault cores (*T* < 11 cm)				**Thick fault cores (*T* > 11 cm)**			
Planar	Breccia	9	9%	Planar	Breccia	4	8%
Planar	Gouge	10	10%	Planar	Cement veins	9	18%
Planar	Cement veins	37	37%	Planar	Shale smear	1	2%
Planar	Shale smear	12	12%	Releasing bend	Cement veins	2	4%
Planar	Composite	6	6%	Fault splay	Breccia	9	18%
Fault bends	Breccia	2	2%	Fault splay	Cement veins	2	4%
Fault bends	Gouge	2	2%	Overlap	Shale smear	1	2%
Fault bends	Composite	1	1%	Overlap	Composite	2	4%
Fault splay	Breccia	1	1%	Overlap	Host rocks	1	2%
Fault splay	Gouge	2	2%	Lenses	Breccia	4	8%
Fault splay	Cement veins	3	3%	Lenses	Composite	6	12%
Fault splay	Shale smear	1	1%	Lenses	Host rocks	8	16%
Fault splay	Composite	2	2%	Lenses	Cement veins	1	2%
Segment link	Cement veins	1	1%				
Segment link	Shale smear	2	2%				
Lenses	Breccia	1	1%				
Lenses	Gouge	2	2%				
Lenses	Calcite	2	2%				
Lenses	Composite	2	2%				
Lenses	Host rocks	2	2%				
Large offset faults (10–50 m disp.)				**All large faults (*N* = 60)**			
Planar	Cement veins	7	16%	Planar	Breccia	5	8%
Planar	Gouge	6	14%	Planar	Cement veins	7	12%
Planar	Breccia	5	11%	Planar	Gouge	6	10%
Planar	Composite	1	2%	Planar	Composite	1	2%
R splay	Breccia	2	5%	R splay	Breccia	2	3%
R' splay	Breccia	4	9%	R′ splay	Breccia	4	7%
Lenses	Breccia	9	20%	Lenses	Breccia	9	15%
Lenses	Host rock lens	5	11%	Lenses	Host rocks	5	8%
Multiple slip	Breccia	5	11%				
Major faults 100–440 disp							
Multiple slip	Breccia	9	56%	Multiple slip	Breccia	14	23%
Multiple slip	Cement veins	3	19%	Multiple slip	Cement veins	3	5%
Multiple slip	Shale smear	2	13%	Multiple slip	Composite	2	3%
Multiple slip	Composite	2	13%	Multiple slip	Shale smear	2	3%

with calcite veins, gouge and shale smear (59%). Another trend is that planar faults hosting breccia membranes and composite facies become more frequent (16%) than for small faults. For the thick faults, lenses consisting of calcite veins, breccias and host rocks combined with composite facies are the most common constituents (38%), whereas the combination of planar fault segments with breccias, calcite veins and shale smear occupies 28% of the dataset.

The *large faults* are analysed in two groups faults with 10–100 m displacement and major faults with more than 100 m displacement (Fig. 11e,f). The reason for this separation is that there is a clear difference in thickness and composition between these two groups, with an average thickness of 43 cm for the faults between 10 and 100 m, and 223 cm for faults with displacement between 100 and 400 m. The separation between thick and localized faults of the

entire dataset is influenced by this difference; smaller displacement large faults occupy the domains of localized faults, whereas the larger displacement faults occupy the thick fault domain. Faults between 10 and 100 m offset have a distributed facies combination; with 41% of the dataset showing planar faults with breccias, gouge and calcite veins. Faults with lenses of breccias and host rocks occupy 31% of the dataset. The remaining data points consist of breccia membranes cut by multiple slip surfaces, or faults geometrically influenced by R splays.

The outcrops of the largest offset faults all display multiple slip surfaces. Faults with a composition of breccias are by the far most common (56%). The remaining faults are composed of composite facies (13%), shale smear (13%), and calcite veins (19%). Fault cores dominated by shale smear occupy the largest thicknesses (3.5 and 11 m).

7. Discussion

7.1. Displacement–thickness relationships

The presented thickness/displacement dataset has a significant scatter of data points (Figs. 10 and 11), revealing up to three orders of magnitude of thicknesses for any given displacement. A similar variation in the thickness/displacement relationships is commonly observed and has been related to varying protoliths, mechanical layering, depth of deformation, fault zone architecture (lenses and anastomosing fracture network), strain widening and localization processes (hardening vs. softening), and observation criteria (Blenkinsop, 1989; Evans, 1990; Shipton et al., 2006; Wibberley et al., 2008; Childs et al., 2009). This variation in thickness offers significant uncertainty for example in the selection of input parameters for reservoir fault seal assessments (Yielding et al., 1997; Manzocchi et al., 1999, 2010; Sperrevik et al., 2002).

We address this variation by further classifying faults into different compositional and geometrical facies, by that exploring some factors controlling the thickness/displacement relationship. Firstly, when comparing small, moderate and large offset faults, the increase in thickness guided by displacement is lower for large faults than for small faults (Fig. 10c). There is also a clear difference in the average thickness/displacement ratio for these three displacement ranges. Contrary to this, most publications addressing thickness/displacement relationships of faults indicate a linear increase in thickness guided by displacement, i.e. the thickness/displacement relationship is similar for all fault scales (e.g. Otsuki, 1978; Robertson, 1983; Scholz, 1987; Hull, 1988; Walsh et al., 1998), which has been ascribed to a constant growth of the fault core controlled by the fault rock rheology and strain hardening (Scholz, 1987; Hull, 1988). Our conclusion is that a power law correlation with an exponent of approximately 0.6 can best represent the general thickness to displacement relationship of fault cores in fine grained carbonates. This trend line agrees with similar datasets, such as that of Shipton et al. (2006), Braathen et al. (2009), Balsamo and Storti (in press), and an unpublished study from fault core thickness in sandstone of Sinai (Braathen and Skar, pers. comm.). The variation in thickness for any given displacement (Fig. 10) can be somewhat reduced by applying two different trend lines; one line representing fault cores with a simple planar geometry and a related simple composition, and a second trend line representing complex, thicker fault cores commonly associated with fault jogs or relay structures, or larger displacement (Fig. 12).

7.2. Fault styles and displacement

A number of studies address fault style in various sedimentary rocks of varying degree of lithification (e.g. Childs et al., 1997; Heynekamp et al., 1999; Agosta and Kirschner, 2003; Storti et al.,

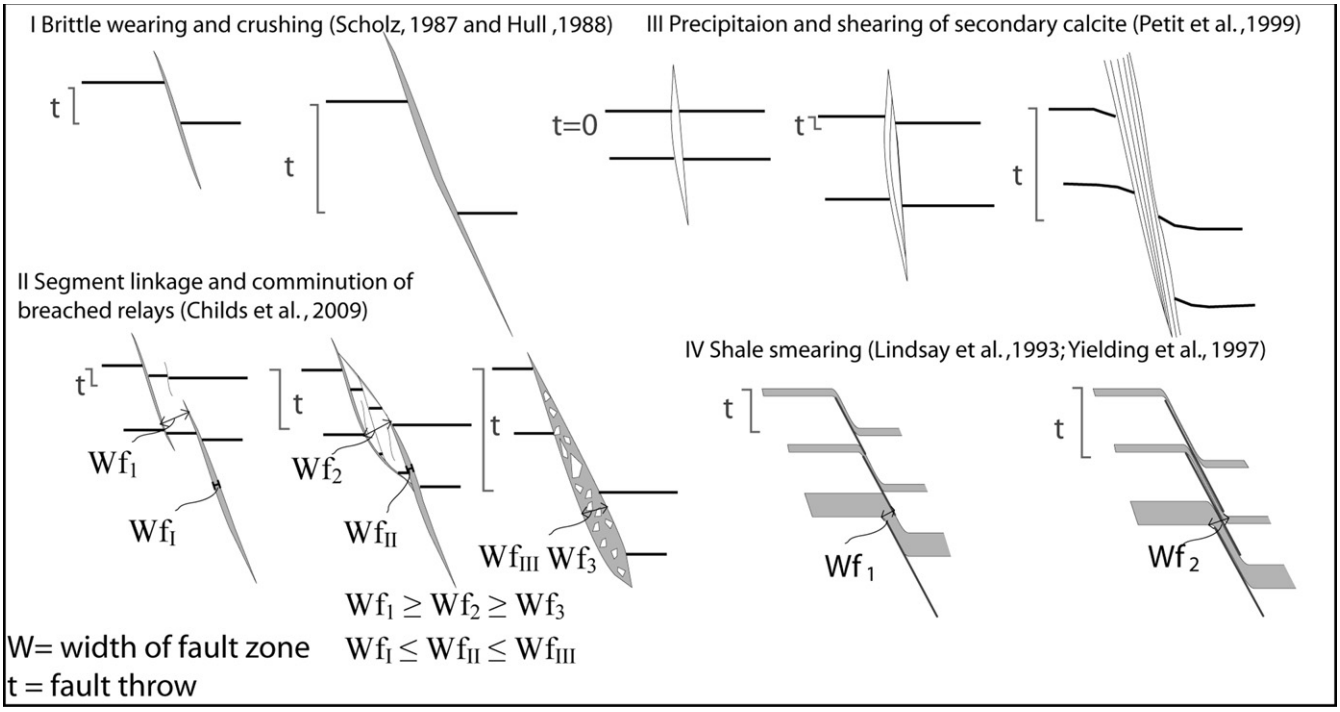

Fig. 12. Schematic representation of stages and mechanism for development of faults in carbonates, based on literature and observations from the three study areas. (i) Increase in thickness due to mechanical hardening of fault rocks related to crushing and frictional wear. (ii) Increase in carbonate fault rock thickness due to linkage, breaching and breakdown of asperities and relay structures. (iii) Increase in calcite vein thickness due to repeated dilational fracturing and precipitation of calcite cement. (iv) Thickening of the core by incorporating several shale layers.

2003; Myers and Aydin, 2004; Labaume et al., 2004; Van der Zee and Urai, 2005; Agosta and Aydin, 2006; Bonson et al., 2007; Benedicto et al., 2008; Braathen et al., 2009; Bastesen et al., 2009). According to Braathen et al. (2009), many of the fault characteristics are recurring and therefore are globally representative, with the distinctive fault zone elements represented by discrete structures, membranes and lenses. Herein, we address the spatial patterns and distribution of these elements in fault cores of fine grained carbonates.

Small offset faults (0,1–1 m) commonly have thin and localized fault cores along straight segments, with membranes consisting of calcite veins, gouge along shear fractures, and shale smear (Figs. 9 and 11). They often reveal linkage of segments where the fault core becomes thicker, but these irregularities show a similar composition as found along the localized segments.

For moderate offset faults (1–10 m), composite cores become more common. Such cores are dominated by both host rock and fault rock lenses surrounded by slip surfaces or slip zones offering both gouge and breccias (Figs. 9 and 11).

For larger faults, a transition exists between 50 m and 100 m of displacement. Faults with 10–50 m offset consist of relatively thin localized membranes of sheared veins and fine grained breccias, and with host rocks lenses similar to moderate offset faults. Larger faults (>100 m offset) show thicker cores with multiple slip zones, hosting significant breccias and shale membranes (Figs. 9 and 11). Further, these cores show extensive calcite precipitation as cement in breccias and in voids, and a prominent development of lenses.

In summary, for fault cores in fine grained carbonates the overall pattern is that of fault initiation dominated by fractures filled with calcite veins and thin shear fractures hosting gouge membranes (Fig. 13). With increased fault offset, complexity increases with breakdown of veins, more extensive fault rock membranes, and a trend towards development of lenses. When offset exceeds 100 m, cores become complex with multiple slip zones, breccia and shale smear membranes, and with lenses. There is also extensive calcite cementation of rocks in the core. This general pattern reflects the development of the fault with repeated activation during accumulation of offset, as discussed below.

7.3. Core development related to fault displacement

Both the temporal and spatial development of fault cores, and the related link to facies composition, is intricate and therefore only possible to discuss in general terms. The observed development in style of extensional fault cores of fine grained carbonate rocks seems influenced by the interplay of – (i) calcite dissolution and precipitation, (ii) disaggregation of rocks (rheology), (iii) shale smearing, and (iv) fault geometry (Figs. 1, 2 and 13).

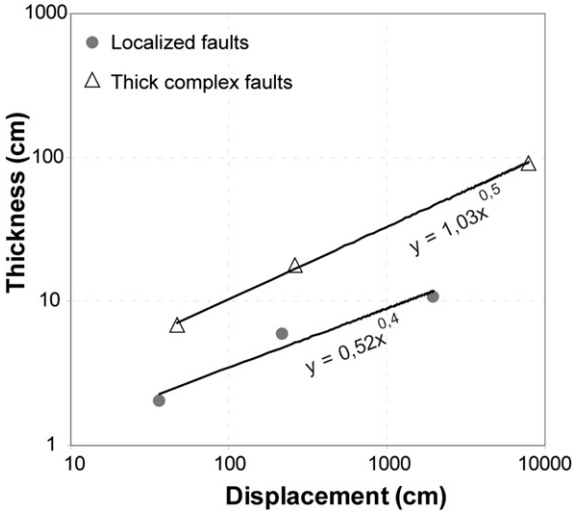

Fig. 13. Average thickness/displacement plot of thick, geometrically-complex fault cores (triangles) and thin localized fault cores (circles). Trend lines are indicated for the two groups.

The dominance of calcite veins in combination with gouge and shale smear observed in the small and moderate offset faults is likely related to the crack seal-slip-mechanism, which may be ascribed to over pressurized fluids in fractures and small faults (Petit et al., 1999). This mechanism is believed to occur in mechanically strong host rocks, where evidence of multiple phases of calcite vein precipitation suggests recurring fracturing and subsequent re-sealing. Repeated slip-surface activation appears to have taken place along the boundary between the host rock and the calcite vein(s), as evidenced by the millimetre thick lenses of host rock limestone and fault gouge surrounded by a crystalline calcite matrix, which are observed along the slip surface. Our study supports Petit et al.'s (1999) conclusion that these veins become less common with increased fault slip, which could mimic higher fluid permeability in larger offset faults. This is based on the observation that the typical crack-seal related veins are common for small faults. For larger faults, the veins become shattered, and lenses of breccia and overlap structures filled with secondary calcite become more common. However, there are contradicting cases; in the Jebel Madar (Oman) area extensive calcite mineralization was found along one of the large faults and similar mineralization is also described for faults and karst caves in the northern part of the Jebel Madar (Montenat et al., 2000; Immenhauser et al., 2007). This extensive calcite precipitation is assumed to be recent; in that dating of calcite from the latter study suggests a Pleistocene age. The secondary calcite is believed to have formed due to mixing of deep-seated fluids with meteoric fluids (Immenhauser et al., 2007). This suggests recent fault (re-)activation and that these faults formed major fluid pathways during their active phases (see also, Roberts and Stewart, 1994 and Bastesen et al., 2009).

Another factor affecting the precipitation of cement is the depth of faulting, which controls the degree of pressure solution (Carrio-Schaffhauser and Gaviglio, 1990; Peacock and Sanderson, 1995; Micarelli et al., 2005; Benedicto et al., 2008). Pressure solution may localize the fault zone, by dissolving carbonate material and leaving insoluble shale gouge along the fault surface (Micarelli et al., 2005; Benedicto et al., 2008). In this study, stylolites are observed between clasts of the core but not along slip surfaces. Further, for large faults, stylolitic surfaces are observed in the damage zones. The fact that many faults experience a high degree of calcite precipitation associated with shale gouge could also be related to pressure solution around insoluble clay. This may explain why carbonates with low shale content have fault cores with thin membranes of shale gouge along slip surfaces, together with sheared calcite veins.

Childs et al. (2009) advocate the link between fault development and fault zone thickness. They show that fault zone width varies from relay structures to fault cores, with the range of thicknesses encountered for relays observed to be as much as seven orders of magnitude higher than for fault cores. Similarly, the fault core thickness is distributed over three orders of magnitude (e.g. Knott, 1994; Sperrevik et al., 2002). To explain this scatter Childs et al. (2009) suggested that the fault is in general weakened by the process of segmental growth of fault arrays due to linkage of fault segments and progressive breakdown to fault rocks. In parallel, the relative thickness is decreasing from un-breached fault segment geometries to fault rock layers. Similar conclusions can be drawn from this study; (i) in general, cores thicken with displacement, and (ii) geometrically-complex faults display thicker cores than individual planar fault segments.

There are, however, changes in the pattern linked to the displacement. Lenses are for instance more common for moderate and large offset faults, contrary to small faults. The observed threshold for lenses between small and moderate offset faults could have several reasons; (i) the "lenses" of small faults are mostly abraded from the walls of slip surfaces and are therefore very small. Thereby, they are observed as rock fragments in gouge rather than as separate elements. (ii) Small faults more commonly consist of isolated segments within a fault array, with fault propagation that is layer/rheology controlled. As these segments link up with increased fault offset, lenses develop in segment linkage areas (Lindanger et al., 2007). At the same time, the fault develops towards a through going structure less affected by wall rock rheology (e.g. Peacock and Sanderson, 1991; Ferrill and Morris, 2003; Schöpfer et al., 2006). As pointed out by Childs et al. (2009), there is no objective means of determining whether a fault-bounded host rock lens was formed by linkage of fault segments and splays or breakdown of asperities and relay structures, in other words related to fault irregularity. But the observed increased likelihood of encountering lenses in larger faults gives general guidelines.

For moderate offset faults (1–10 m), composite fault cores become more common. This could relate to shale layers that are dragged along the fault and become juxtaposed with pre-existing calcite veins and breccias. Alternatively, the smears are developed in segment overlaps by shale layer rotation perhaps in parallel with disintegration of stronger rocks into breccias along the slip zones. Another trend is that the moderate offset faults have breccias that form lenses/pockets, not through going membranes as commonly found in large offset faults. This could be explained by the breakdown and disintegration of lenses with given positions within the core, which results in localized breccias. Along a similar line, breccias could relate to segment and splay linkage causing direct disintegration of (strong) rocks in linkage areas. With increasing offset, the development of the fault rocks in the core connects to the number of disintegrated lenses and shattered linkage/irregularity areas. If lenses and irregularities appear throughout the fault evolution, the fault rocks would gradually become more widespread and thereby start to form a multi-layer, progressively more continuous membrane along the fault core. Further, the same fault rocks would experience rejuvenation during fault events, developing internal thin shear zones or slip zones, hosting finer grained fault rocks that surround fault rock lenses. These shear zones commonly thin the fault rocks membranes. Both the shear zones in fault rocks and the thinning of such rocks are frequently observed in this study for faults with displacement between 10 and 100 m.

For faults with an offset exceeding 100 m, the common characteristics is that of thicker cores with multiple slip zones and/or slip surfaces, significant breccia and shale membranes, and a prominent occurrences of lenses. In that lenses are common for the large offset faults, the process of lens formation and lens and fault irregularity breakdown seems continuous through the fault evolution, as envisioned by Childs et al. (2009).

One exception to this is some extensional faults formed in anticlines of Oman. There, faults show thick breccias for relatively small displacements, which could relate to dilation across the crest of anticlines at shallow level in the crust (Ferrill and Morris, 2003). This illustrates that the forces (extension, compression) acting in the fault core could influence both the core thickness and its intrinsic composition. However, the fault core characteristics are probably experiencing a stronger guidance by the mechanical heterogeneity of wall rocks, especially for smaller offsets. With increasing offset and better developed fault cores, the core lithologies and their developing rheology would also contribute (e.g. Peacock and Sanderson, 1991; Schöpfer et al., 2006; Childs et al., 2009). Finally, geometric effects arising from fault irregularities, splaying and segmentation would be an important factor.

8. Conclusions

This work addresses the relationship between thickness and displacement of fault cores in fine grained carbonates. We relate this relationship to the fault geometry, and the fault core and host rock lithology:

1) Fault in fine grained carbonates has geometries varying between simple fault cores and fault cores comprising fault splays, lenses, segment linkages and overlap structures.
2) Typical rocks representing the thickness of the fault core are carbonate breccias, carbonate and shale gouge, shale smear, secondary calcite cement and veins, and host rock lenses.
3) There is a large scatter in fault core thickness vs. displacement. Generally, the fault core thickness increases with displacement that may be expressed by a power law function ($0.29D^{0.56}$). This trend describes a gradual decrease in the thickness/displacement relationship for increasing slip along faults. In more detail, the general function is the sum of two (power law) trend lines; the first representing thin localized fault cores with generally simple and planar geometry, the second representing thicker fault cores with complex geometry of lenses and overlap structures and with rock membranes.
4) There is a significant change in composition and geometry from small (0–1 m), to moderate (1–10 m) and to large offset faults (10–400 m).
   - Small faults have thin, localized fault cores along straight segments, with membranes consisting of calcite veins, gouge along shear fractures, and shale smear. They often reveal thicker segment linkage areas with a similar composition.
   - Moderate faults commonly have composite cores dominated by both host rock and fault rock lenses surrounded by slip surfaces or slip zones with gouge and breccias.
   - Large faults with 50 m and 100 m offset consist of relatively thin localized membranes of sheared veins and fine grained breccias, and with host rocks lenses. In contrast, larger faults (>100 m offset) show thicker cores with multiple slip zones, long breccia and shale membranes that often are cemented, and lenses.
5) We envision that fault development is guided by forces (extension, compression) acting in the fault, mechanical heterogeneity of wall rocks, the core lithologies and their developing rheology, and geometric effects arising from fault irregularities.

Acknowledgement

Ian Sharp and David Hunt are gratefully thanked for providing excellent maps and for introducing us to the Sinai and Oman field areas. The manuscript benefitted significantly through critical review of Fabrizio Balsamo and Roger Soliva. Roy H. Gabrielsen, Atle Rotevatn, Jan Tveranger and Simon Buckley are thanked for great efforts in reviewing and discussing the paper. For field companionship and exceptionally insightful discussions the authors wish to thank Haakon and Sigurd Fossen, Harmon Maher, Sylvie Schueller and Walter Wheeler.

The study was financed by the Fault Facies project at the Centre for Integrated Petroleum Research, University of Bergen, by support from ConocoPhillips, StatoilHydro, the Research Council of Norway, and the University Centre on Svalbard.

References

Agosta, F., Kirschner, D.L., 2003. Fluid conduits in carbonate hosted seismogenic normal faults of central Italy. Journal of Geophysical Research 108 (No B4), 13.

Agosta, F., Aydin, A., 2006. Architecture and deformation mechanism of a basin-bounding normal fault in Mesozoic platform carbonates, central Italy. Journal of Structural Geology 28 (8), 1445–1467.

Al-Kindi, M., Casey, M., Butler, R.W.H., 2006. Structural evolution and fracture patterns in front range of northern Oman Mountains. In: Middle East Conference and Exhibition Manama, Bahrain.

Alsharhan, A.S., Nairn, A.E., 1997. M. Sedimentary Basins and Petroleum Geology of the Middle East. Elsevier, Amsterdam, pp. 843.

Alsharhan, A.S., 2003. Petroleum geology and potential hydrocarbon plays in the Gulf of Suez rift basin, Egypt. American Association of Petroleum Geologists 87, 143–180.

Balsamo, F., Storti, F. Grain size and permeability evolution of soft-sediment extensional sub-seismic and seismic fault zones in high-porosity sediments from the Crotone basin, southern Apennines, Italy. Marine and Petroleum Geology, in press.

Bastesen, E., Braathen, A., Nøttveit, H., Gabrielsen, R.H., Skar, T., 2009. Extensional fault cores in micritic carbonates, a case study from Gulf of Corinth, Greece. Journal of Structural Geology 31, 403–420.

Benedicto, A., Plagnes, V., Vergély, P., Flotté, N., Schultz, R.A., 2008. Fault and fluid interaction in a rifted margin: integrated study of calcite-sealed fault-related structures (Southern Corinth margin). In: Wibberley, C.A.J., Kurz, W., Imber, J., Holdsworth, R.E., Collettini, C. (Eds.), The Internal Structure of Fault Zones: Implications for Mechanical and Fluid-Flow Properties. Geological Society, London, Special Publications, vol. 299, pp. 257–275.

Billi, A., Salvini, F., Storti, F., 2003. The damage zone fault core transition in carbonate rocks: implications for fault growth, structure and permeability. Journal of Structural Geology 25, 1779–1794.

Billi, A., 2005. Grain size distribution and thickness of breccia and gouge zones from thin (<1 m) strike-slip fault cores in limestone. Journal of Structural Geology 27, 1823–1837.

Blenkinsop, T.G., 1989. Thickness–displacement relationships for deformation zones: discussion. Journal of Structural Geology 11, 1051–1054.

Bonson, C.G., Childs, C., Walsh, J.J., Schopfer, M.P.J., Carboni, V., 2007. Geometric and kinematic controls on the internal structure of a large normal fault in massive limestones: the Maghlaq Fault, Malta. Journal of Structural Geology 29 (2), 336–354.

Bosworth, W., Huchon, P., McClay, K., 2005. The Red Sea and Gulf of Aden Basins. Journal of African Earth Sciences 43 (1–3), 334–378.

Braathen, A., Osmundsen, P.T., Gabrielsen, R.H., 2004. Dynamic development of fault rocks in a crustal-scale detachment: an example from western Norway. Tectonics 23 (No. 4 TC4010), 1–21.

Braathen, A., Tveranger, J., Fossen, H., Skar, T., Cardozo, N., Semshaug, S.L., Bastesen, E., Sverdrup, E., 2009. Fault facies and its applications to sandstone reservoirs. American Association of Petroleum Geologists Bulletin 93, 891–917.

Caine, J.S., Evans, J.P., Forster, C.B., 1996. Fault zone architecture and permeability structure. Geology 24, 1025–1028.

Carrio-Schaffhauser, E., Gaviglio, P., 1990. Pressure solution and cementation stimulated by faulting in limestones. Journal of Structural Geology 12 (8), 987–994.

Cello, G., Tondi, E., van Dijk, J.P., Mattioni, L., Micarelli, L., Pinti, S., 2003. Geometry, kinematics and scaling properties of faults and fractures as tools for modelling geofluid reservoirs: Examples from the Appennines, Italy. In: Niewland, D.A. (Ed.), New Insights into Structural Interpretation and Modelling. Geological Society, London, Special Publications, vol. 212, pp. 7–22.

Chester, F.M., Logan, J.M., 1986. Composite planar fabric of gouge from the Punchbowl fault zone, California. Journal of Structural Geology 9, 621–634.

Childs, C., Watterson, J., Walsh, J.J., 1996. A model for the structure and development of fault zones. Journal of the Geological Society of London 153, 337–340.

Childs, C., Walsh, J.J., Watterson, J., 1997. Complexity in fault zone structure and implications for fault seal prediction. In: Møller-Pedersen, P., Koestler, A.G. (Eds.), Hydrocarbon Seals: Importance for Exploration and Production. Norwegian Petroleum Society Special Publication, vol. 7, pp. 61–72.

Childs, C., Manzocchi, T., Walsh, J.J., Bonson, C.G., Nicol, A., Schöpfer, M.P.J., 2009. A geometric model of fault zone and fault rock thickness variations. Journal of Structural Geology 31 (2), 117–127.

Eliassen, A., Talbot, M.R., 2003. Sedimentary facies and depositional history of the mid Carboniferous Minkinfjellet Formation, central Spitsbergen. Norwegian Journal of Geology 83, 299–318.

Evans, J.P., 1990. Thickness–displacement relationships for fault zones. Journal of Structural Geology 12 (8), 1061–1065.

Ferrill, D.A., Morris, A.P., 2003. Dilational normal faults. Journal of Structural Geology 25 (2), 183–196.

Gabrielsen, R.H., Clausen, J.A., 2001. Horses and duplexes in extensional regimes: a scale modelling contribution. In: Koyi, H.A., Mancktelow, N.S. (Eds.), Tectonic Modeling: A Volume in Honor of Hans Ramberg. Geological Society of America Memoir 193, pp. 219–233.

Graham Wall, B.R., Girbacea, R., Mesonjesi, A., Aydin, A., 2006. Evolution of fracture and fault controlled fluid pathways in carbonates of the Albanides fold and thrust belt. American Association of Petroleum Geologists Bulletin 90, 1227–1249.

Grélaud, C., Razin, P., Homewood, P.W., Schwab, A.M., 2006. Development of incisions on a periodically emergent carbonate platform (Natih Formation late Cretaceous Oman). Journal of Sedimentary Research 76, 647–669.

Hanna, S.S., 1990. The Alpine deformation of the CentralOman Mountains. In: Geological Society, London, Special Publications, vol. 49, pp. 341–359.

Heynekamp, M.R., Goodwin, L.B., Mozley, P.S., Haneberg, W.C., 1999. Controls on fault-zone architecture in poorly lithified sediments, Rio Grande Rift, New Mexico: implications for fault-zone permeability and fluid flow. In: Goodwin, L.B., Mozley, P.S., Moore, J.M., Haneberg, W.C. (Eds.), Faults and Subsurface Fluid Flow in the Shallow Crust. Geophysical Monograph 113. American Geophysical Union, Washington, pp. 27–49.

Hull, J., 1988. Thickness–displacement relationships for deformation zones. Journal of Structural Geology 10, 431–435.

Immenhauser, A., Dublyansky, Y.V., Verwer, K., Fleitman, D., Pashenko, S.E., 2007. Textural, elemental and isotopic characteristics of Pleistocene phreatic cave deposits (Jabal Madar, Oman). Journal of Sedimentary Research 77, 68–88.

Jackson, C.A.L., Gawthorpe, R.L., Leppard, C.W., Sharp, I.R., 2006. Rift-initiation development of normal fault blocks: insights from the Hammam Faraun fault block, Suez Rift, Egypt. Journal of the Geological Society 163 (1), 165–183.

Johannessen, E.P., Steel, R., 1992. Mid-carbonferous extension and rift-infill sequences in the Billefjorden through, Svalbard. Norsk Geologisk Tidskrift 72, 35–48.

Knott, S.D., 1994. Fault zone thickness versus displacement in the Permo-Triassic sandstones of NW England. Journal of the Geological Society 151, 17–25.

Kuss, J., Scheiber, C., Gietl, R., 2000. Carbonate platform to basin transition along an Upper Cretaceous to Lower Tertiary Syrian Arc uplift, Galala Plateaus, Eastern Desert of Egypt. GeoArabia 5, 405–424.

Labaume, P., Carrio-Schaffhauser, E., Gamond, J.-F., Renard, F., 2004. Deformation mechanisms and fluid-driven mass transfers in the recent fault zones of the Corinth Rift (Greece). Comptes Rendus Geosciences 336 (4–5), 375–383.

Lindanger, M., Gabrielsen, R.H., Braathen, A., 2007. Analysis of rock lenses in extensional faults. Norwegian Journal of Geology 87, 361–372.

Lindsay, N.G., Murphy, F.C., Walsh, J.J., Watterson, J., 1993. Outcrop studies of shale smears on fault surfaces. In: Flint, S.S., Bryant, I.D. (Eds.), The Geological Modelling of Hydrocarbon Reservoirs and Outcrop Analogues. Special Publications, International Association of Sedimentologists, vol. 15, pp. 113–123.

Maher, H.D. Jr., Braathen, A. Løvehovden fault and Billefjorden rift basin segmentation and development, Spitsbergen. Geological Magazine, in press.

Manzocchi, T., Walsh, J.J., Nell, P., Yielding, G., 1999. Fault transmissibility multipliers for flow simulation models. Petroleum Geoscience 5, 53–63.

Manzocchi, T., Childs, C., Walsh, J.J., 2010. Faults and fault properties in hydrocarbon flow models. Geofluids 10, 94–113.

McCann, A.J., Dallmann, W.K., 1996. Reactivation history of the long-lived Billefjorden Zault Zone in the north Central Spitsbergen, Svalbard. Geological Magazine 133, 63–84.

Micarelli, L., Moretti, I., Daniel, J.M., 2003. Structural properties of rift-related normal faults: the case study of the Gulf of Corinth, Greece. Journal of Geodynamics 36 (1–2), 275–303.

Micarelli, L., Benedicto, A., Invernizzi, C., Saint-Bezar, B., Michelot, J.L., Vergely, P., 2005. Influence of P/T conditions on the style of normal fault initiation and growth in limestones from the SE-Basin, France. 2006. Journal of Structural Geology 27, 1577–1598.

Micarelli, L., Benedicto, A., Wibberley, C.A.J., 2006. Structural evolution and permeability of normal fault zones in highly porous carbonate rocks. Journal of Structural Geology 28 (7), 1214–1227.

Montenat, C., Soudet, H.J., Barrier, P., Cherau, A., 2000. Karstification and tectonic evolution of the Jabal Madar (Adam Foothills, Arabian platform) during the Upper Cretaceous Bulletin Centre de Recherches. ELF Exploration Production 22, 161–183.

Moustafa, A.R., Abdeen, M.M., 1992. Structural setting of the Hamman Faraoun block, eastern side of the Suez rift. Journal of the University of Kuwait (Science) 19, 291–309.

Moustafa, A.R., 2004. Geologic maps of the eastern side of the Suez Rift (Western Sinai Peninsula), Egypt. American Association of Petroleum Geologists Map Series.

Myers, R., Aydin, A., 2004. The evolution of faults formed by shearing across joint zones in sandstone. Journal of Structural Geology v. 26, 947–966.

Otsuki, K., 1978. On the relationship between the width of shear zone and the displacement along fault. Journal of the Geological Society of Japan 84, 661–669.

Patton, T.L., Moustafa, A.R., Nelson, R.A., Abdine, S.A., 1994. Tectonic evolution and structural setting of the Suez Rift. In: Landon, S.M. (Ed.), Interior Rift Basin American Association of Petroleum Geologists Memoir 59, pp. 7–55.

Peacock, D.C.P., Sanderson, D.J., 1991. Displacements, segment linkage and relay ramps in normal fault zones. Journal of Structural Geology 13, 721–733.

Peacock, D.C.P., Sanderson, D.J., 1995. Pull aparts, shear fractures and pressure solution. Tectonophysics 241, 1–13.

Peacock, D.C.P., 2002. Propagation, interaction and linkage in normal fault systems. Earth Science Reviews 58 (1–2), 121–142.

Petit, J.P., 1987. Criteria for the sense of movement on fault surfaces in brittle rocks. Journal of Structural Geology 9 (5–6), 597–608.

Petit, J.-P., Wibberley, C.A.J., Ruiz, G., 1999. 'Crack-seal', slip: a new fault valve mechanism? Journal of Structural Geology 21 (8–9), 1199–1207.

Pickard, N.A.H., Eilertsen, F., Hanken, N.M., Johansen, T.A., Lønøy, A., Nakrem, H.A., Nilsson, I., Samuelsberg, T.J., Somerville, I., 1996. Stratigraphic framework of upper

Carboniferous (Moscovian-Kasimovian) strata in BünsowLand. Central Spitsbergen: palaeogeographic implications. Norsk Geologisk Tidskrift 76, 169–185.
Putz-Perrier, M.W., Sanderson, D.J., 2010. Distribution of faults and extensional strain in fractured carbonates of the North Malta Graben. American Association of Petroleum Geologists 94 (No 4), 435–456.
Roberts, G., Stewart, I., 1994. Uplift, deformation and fluid involvement within an active normal fault zone in the Gulf of Corinth, Greece. Journal of the Geological Society of London 151, 531–541.
Robertson, E.C., 1983. Relationship of fault displacement to gouge and breccia thickness. Mining Engineering 35, 1426–1432.
Robson, D.A., 1971. The structure of the Gulf of Suez (Clysmic) rift, with special reference to the eastern side. Journal of the Geological Society 127 (3), 247–271.
Rykkelid, E., Fossen, H., 2002. Layer rotation around vertical fault overlap zones: observations from seismic data, field examples, and physical experiments. Marine and Petroleum Geology 19 (2), 181–192.
Said, R., 1960. Planktonic foraminafera from the Thebes formation, Luxor, Egypt. Micropaleontology 6 (3), 277–286.
Samuelsberg, T., Elvebakk, G., Stemmerik, L., 2003. Late Palaeozoic evolution of the Finnmark platform, southern Norwegian Barents Sea. Norwegian Journal of Geology 83, 351–362.
Scholz, C.H., 1987. Wear and gouge formation in brittle faulting. Geology 15, 493–495.
Scott, R.W., 1990. Chronostratigraphy of the Cretaceous carbonate shelf, southeastern Arabia. In: Geological Society, London, Special Publications, vol. 49, pp. 89–108.
Schöpfer, M.P.J., Childs, C., Walsh, J.J., 2006. Localisation of normal faults in multilayer sequences. Journal of Structural Geology 28, 816–833.
Sharp, I.R., Gawthorpe, R.L., Armstrong, B., Underhill, J.R., 2000. Propagation history and passive margin rotation of mesoscale normal faults: implications for synrift stratigraphic development. Basin Research 12, 285–305.
Shipton, Z.K., Soden, A.M., Kirkpatrick, J.D., Bright, A.M., Lunn, R.J., 2006. How thick is a fault? Fault displacement–thickness scaling revisited. In: Abercrombie, R., McGarr, A., Di Toro, G., Kanamori, H. (Eds.), Radiated Energy and the Physics of Faulting. American Geophysical Union Monograph Series 170, pp. 193–198.
Sibson, R.H., 1977. Fault rocks and fault mechanisms. Jornal of the Geological Society of London 133, 191–213.
Soliva, R., Benedicto, A., 2005. Geometry scaling relations and spacing of vertically restricted normal faults. Journal of Structural Geology 27, 317–325.
Steel, R.J., Worsley, D., 1984. Svalbard`s post Caledonian strata – an atlas on sedimentational patterns and palaeogeographic evolution. In: Graham and Trotman, Petroleum Geology of the North European Margin. Norwegian Petroleum Society, pp. 109–135.
Storti, F., Billi, A., Salvini, F., 2003. Particle size distributions in natural carbonate fault rocks: insights for non-self-similar cataclasis. Earth and Planetary Science Letters 206 (1–2), 173–186.
Sperrevik, S., Gillespie, P.A., Fisher, Q.J., Halvorsen, T., Knipe, R.J., 2002. Empirical estimation of fault rock properties. In: Koestler, A.G., Hunsdale, R. (Eds.), Hydrocarbon Seal Quantification. Norwegian Petroleum Society, Special Publication, vol. 11, pp. 109–125.
Tveranger, J., Braathen, A., Skar, T., Skauge, A., 2005. Centre for Integrated Petroleum Research – research activities with emphasis on fluid flow in fault zones. Norwegian Journal of Geology 85, 63–71.
Van der Zee, W., Urai, J.L., 2005. Processes of normal fault evolution in a siliciclastic sequence: a case study from Miri, Sarawak, Malaysia. Journal of Structural Geology 27, 2281–2300.
Wagner, P.D., 1990. Geochemical stratigraphy and porosity controls in cretaceous carbonates near the Oman Mountains. In: Geological Society, London, Special Publications, vol. 49, pp. 127–137.
Walsh, J., Watterson, J., Heath, A.E., Childs, C., 1998. Representation and scaling of faults in fluid flow models. Petroleum Geoscience 4, 241–251.
Wibberley, C.A.J., Yielding, G., Di Toro, G., 2008. Recent advances in the understanding of fault zone internal structure: a review. In: Wibberley, C.A.J., Kurz, W., Imber, J., Holdsworth, R.E., Collettini, C. (Eds.), The Internal Structure of Fault Zones: Implications for Mechanical and Fluid-Flow Properties. Geological Society of London, Special Publication, vol. 299, pp. 5–33.
Yielding, G., Freeman, B., Needham, D.T., 1997. Quantitative fault seal prediction. American Association of Petroleum Geologists Bulletin 81, 897–917.